
DISENTANGLING TOTAL-VARIANCE AND SIGNAL-TO-NOISE-RATIO IMPROVES DIFFUSION MODELS

**Khaled Kahouli^{*1,2}, Winfried Ripken^{1,2}, Stefan Gugler^{1,2}, Oliver T. Unke⁵,
Klaus-Robert Müller^{1,2,3,4,5}, and Shinichi Nakajima^{1,2,6}**

¹BIFOLD – Berlin Institute for the Foundations of Learning and Data

²Machine Learning Group, Technische Universität Berlin

³Department of Artificial Intelligence, Korea University

⁴Max-Planck Institute for Informatics

⁵Google DeepMind

⁶RIKEN Center for Advanced Intelligence Project

ABSTRACT

The long sampling time of diffusion models remains a significant bottleneck, which can be mitigated by reducing the number of diffusion time steps. However, the quality of samples with fewer steps is highly dependent on the noise schedule, i.e., the specific manner in which noise is introduced and the signal is reduced at each step. Although prior work has improved upon the original variance-preserving and variance-exploding schedules, these approaches *passively* adjust the total variance, without direct control over it. In this work, we propose a novel total-variance/signal-to-noise-ratio disentangled (TV/SNR) framework, where TV and SNR can be controlled independently. Our approach reveals that schedules where the TV explodes exponentially can often be improved by adopting a constant-TV schedule while preserving the same SNR schedule. Furthermore, generalizing the SNR schedule of the optimal transport flow matching significantly improves the generation performance. Our findings hold across various reverse diffusion solvers and diverse applications, including molecular structure and image generation.

1 Introduction

With the development of diffusion models [Sohl-Dickstein et al., 2015, Ho et al., 2020, Song and Ermon, 2020, Song et al., 2021a], generative modeling has witnessed great progress in recent years. They have demonstrated remarkable capabilities across various traditional domains such as image synthesis [Dhariwal and Nichol, 2021, Nichol et al., 2022, Rombach et al., 2022, Peebles and Xie, 2023, Ma et al., 2024] and audio generation [Kong et al., 2021, Chen et al., 2021, Liu et al., 2023a]. In computational chemistry, diffusion models have been increasingly utilized as an efficient alternative for tasks like molecule generation [Gebauer et al., 2022, Hoogeboom et al., 2022, Wu et al., 2022, Huang et al., 2023, Xu et al., 2023, Peng et al., 2023, Vignac et al., 2023, Le et al., 2024], relaxation [Kahouli et al., 2024], and conformer search [Xu et al., 2022].

Despite their superior generative capabilities, such as achieving state-of-the-art Fréchet Inception Distance (FID) scores in image generation, diffusion models are computationally expensive during inference. Generating samples requires iteratively solving a reverse stochastic process, where a learned *score function*, generally a deep neural network, must be evaluated at each step. Therefore, reducing the sampling cost without degrading the sample quality requires solving the reverse process with minimal score function evaluations while avoiding high discretization errors. To address this challenge, prior work has explored both training-based improvements [Nichol and Dhariwal, 2021, Watson et al., 2022, Salimans and Ho, 2022, Song et al., 2023a, Lu and Song, 2025, Kim et al., 2025] and advanced sampling techniques, including higher-order solvers, to replace conventional first-order methods [Lu et al., 2022a, Liu et al., 2022, Dockhorn et al., 2022, Jolicoeur-Martineau et al., 2022, Zheng et al., 2023, Zhang and Chen, 2023, Zhao et al., 2023]. Moreover, the critical role of the noise schedule in determining the performance of diffusion models was highlighted in previous work [Chen, 2023, Lin et al., 2024]. Complementary to these approaches, the seminal work of Karras et al. [2022] introduced EDM, which modifies the reverse

^{*}correspondence to khaled.kahouli@tu-berlin.de

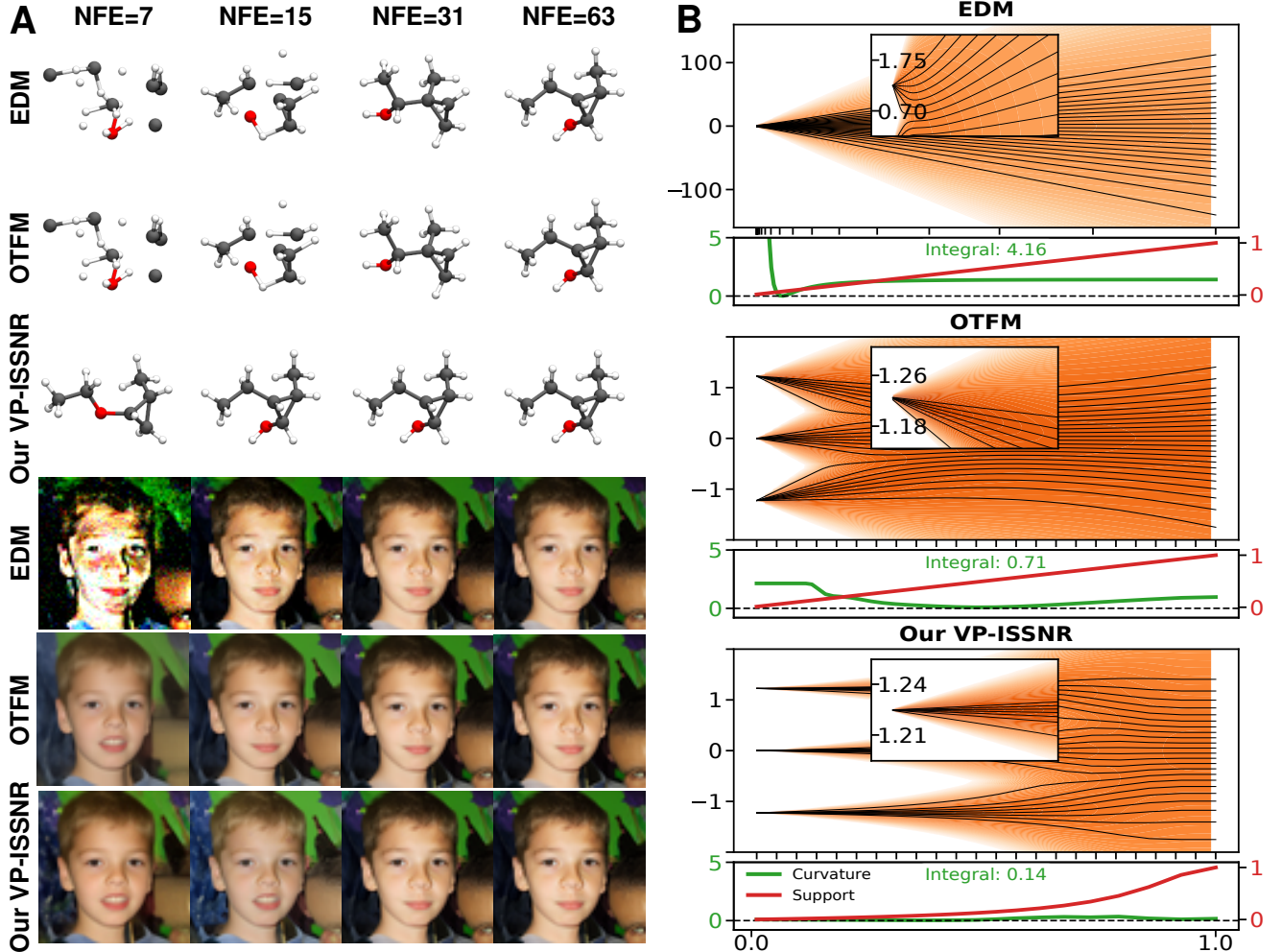


Figure 1: **A:** Our VP-ISSNR schedule enables the generation of stable molecules (top) with diffusion models using far fewer numbers of function evaluations (NFEs) than established methods like EDM and OTFM. It also converges to visually appealing images (bottom) faster than the optimized EDM sampler, and comparably to OTFM. **B:** A numerical analysis of ODE trajectories reveals that our proposed VP-ISSNR schedule has both low trajectory curvature (green curves) and sufficiently large support of marginal distributions (red curves), which are required for high sample generation quality with small NFEs (see Section 4.3).

process to follow straighter trajectories and employs a non-uniform time grid to reduce discretization errors. Additionally, by leveraging a second-order ODE solver, EDM further enhances both sampling efficiency and quality. Building on the concept of straight paths in probability flows, flow matching was proposed as a simulation-free approach to train continuous normalizing flows and as a generalization of diffusion models [Liu et al., 2023b, Lipman et al., 2023]. In this framework, the particular case of linear interpolation by using optimal transport as a conditional probability path has been explored to enforce straight ODE trajectories [Albergo and Vanden-Eijnden, 2023, Pooladian et al., 2023, Tong et al., 2024]. Flow matching has also been successfully applied to molecules [Klein et al., 2023, Song et al., 2023b, Irwin et al., 2024].

Given a data sample $\mathbf{x}(0)$, the forward diffusion process employing a standard Wiener process can be modeled with a time-dependent perturbation kernel:

$$p(\mathbf{x}(t)|\mathbf{x}(0)) = \mathcal{N}(\mathbf{x}(t); a(t)\mathbf{x}(0), b^2(t)\mathbf{I}), \quad (1)$$

where $t \in [0, 1]$, $a(t)$ controls the signal strength, $b(t)$ controls the noise level at each diffusion step, and \mathbf{I} denotes the identity matrix. $a(t)$ and $b(t)$ are smooth non-negative functions that satisfy the following conditions: for small Δt , $a(\Delta t) \approx 1$ and $b(\Delta t) \approx 0$, ensuring that $\mathbf{x}(\Delta t) \approx \mathbf{x}(0)$. Additionally, $a(1) \ll b(1)$ to ensure that $\mathbf{x}(1)$ follows an isotropic Gaussian distribution. Diffusion processes can be roughly categorized into variance-preserving (VP) [Ho et al., 2020] and variance-exploding (VE) [Song and Ermon, 2019] variants, each corresponding to specific choices of $a(t)$ and $b(t)$, determined by a

pre-defined noise schedule. For example, EDM adopts the VE variant with $a(t) = 1$ and $b(t) = t$, achieving state-of-the-art performance in diffusion-based image generation.

In this paper, we aim to further improve noise scheduling by introducing a total-variance/signal-to-noise ratio (TV/SNR) disentangled framework, where the TV defined as $\tau^2(t) = a^2(t) + b^2(t)$, and the SNR as $\gamma(t) = a(t)/b(t)$ [Kingma et al., 2021] are independently controlled. The reverse process is then solved using the corresponding ODE/SDE.

Our empirical results indicate that fast sample generation of scheduling methods with exponentially growing TV can be significantly improved by modifying the TV schedule to instead follow a VP trajectory (i.e., $\tau(t) = 1$), while keeping the SNR schedule $\gamma(t)$ unchanged (see Figure 3 left). Based on this observation, we hypothesize that a constant TV schedule ($\tau(t) = 1$) is already a sufficiently effective choice. Therefore, instead of fully exploring all possibilities of more sophisticated TV schedules, we focus on optimizing the SNR schedule. Specifically, we propose an exponential inverse sigmoid (IS) function for scheduling the SNR (ISSNR), which allows rapid SNR decay both at the beginning ($t \approx 0$) and the end ($t \approx 1$) of the diffusion process. The ISSNR schedule can be seen as a generalization of optimal transport flow matching (OTFM), and achieves state-of-the-art (SOTA) sampling efficiency in molecular structure generation. As shown in Figure 1, we observe a similar tendency in image generation tasks, where our ISSNR schedule performs comparably to SOTA methods. Based on a numerical analysis of ODE trajectories (see Section 4.3), we hypothesize the effectiveness of our approach is due to low curvature of trajectory paths when $t \ll 1$, meaning *close to the data space*, and the time evolution of the marginal distribution. This offers new insights into fast sample generation using diffusion models. Our source code can be accessed at <https://github.com/khaledkah/tv-snr-diffusion>.

The key contributions of our paper are:

- We introduce a novel TV/SNR disentangled framework, where TV and SNR are independently controlled. Many existing diffusion models can be reformulated within this unifying framework (see Table A1 in Appendix A).
- We empirically show that for both molecular structure and image generation tasks, sample generation performance of common schedules with exponential TV growth can be significantly improved by transforming them into their VP counterparts within our framework.
- We propose to schedule the SNR using an exponential inverse sigmoid function (ISSNR schedule), which shows improved sampling performance across various reverse diffusion solvers and different modalities (images and molecules).
- We numerically analyze the curvature of ODE trajectories near the data space and the time evolution of marginal distribution paths, and discuss their importance for fast sampling.

2 Background

2.1 Diffusion Models

Let $p_{\text{data}}(\mathbf{x}(0))$ be the data distribution of interest defined on the support $\mathcal{X} \subseteq \mathbb{R}^d$. We assume that the data are standardized, i.e., $\mathbb{E}_{p_{\text{data}}}[\mathbf{x}(0)] = \mathbf{0}$ and $\text{Var}_{p_{\text{data}}}[\mathbf{x}(0)] = \mathbf{1}$. Let $\{\mathbf{x}(t)\}_{t \in [0,1]}$ be the forward diffusion process describing the stochastic flow of the marginal probability density path $\{p_t(\mathbf{x})\}_{t \in [0,1]}$ resulting from iterative injection of Gaussian noise (starting from $p_0 := p_{\text{data}}$ and ending at a tractable Gaussian prior $p_1(\mathbf{x})$). Once we define the perturbation kernel in Eq. (1), the marginal density path for $t \in [0, 1]$ is fixed as

$$p_t(\mathbf{x}(t)) = \int p(\mathbf{x}(t) | \mathbf{x}(0)) p_{\text{data}}(\mathbf{x}(0)) \, d\mathbf{x}(0), \quad (2)$$

and the corresponding SDE is

$$\begin{aligned} d\mathbf{x} &= \mathbf{x}f(t)dt + g(t)d\mathbf{w}, \quad \text{where} \\ f(t) &= \frac{\dot{a}(t)}{a(t)} \quad \text{and} \quad g(t) = \sqrt{2\frac{b(t)}{a(t)} \left(a(t)\dot{b}(t) - \dot{a}(t)b(t) \right)}. \end{aligned} \quad (3)$$

Here, \mathbf{w} is the standard Wiener process and $f(t)$ and $g(t)$ are the drift and diffusion coefficients, respectively. We use Newton's notation for time derivatives, e.g., $\dot{a}(t) = \frac{d}{dt}a(t)$.

The reverse SDE for Eq. (3) is given by

$$d\tilde{\mathbf{x}} = \left[\tilde{\mathbf{x}}f(t) - \frac{1 + \lambda^2}{2}g(t)^2 \nabla_{\tilde{\mathbf{x}}} \log p_t(\tilde{\mathbf{x}}) \right] d\tilde{t} + \lambda g(t) d\tilde{\mathbf{w}} \quad (4)$$

for $\lambda = 1$, where the tilde indicates time-reversal, i.e., $\tilde{t} = 1 - t$, and $\nabla_{\mathbf{x}} \log p_t(\mathbf{x})$ is the score function of the marginal density at time t . Eq. (4) describes the general reverse SDE for $\lambda \geq 0$, including the ones with less ($\lambda < 1$) or more ($\lambda > 1$) stochasticity with the same marginal distribution. The extreme case where $\lambda = 0$ corresponds to the probability flow ODE [Zhang and Chen, 2021].

Training diffusion models amounts to approximating the unknown score function of the marginal density in Eq. (2) for $t = [0, 1]$ by a parametrized neural network, $\mathbf{s}_\theta(\mathbf{x}(t), t) \approx \nabla_{\mathbf{x}} \log p_t(\mathbf{x})$. The parameters can be fitted by a re-weighted version of denoising score-matching (DSM) [Vincent, 2011, Song and Ermon, 2019, Song et al., 2021a]:

$$\theta^* = \operatorname{argmin}_\theta \mathbb{E}_{p_{\text{data}}(\mathbf{x}(0))} \mathbb{E}_{p(\mathbf{x}(t)|\mathbf{x}(0))} [\|\varepsilon_t - \varepsilon_\theta(\mathbf{x}(t), t)\|^2], \quad (5)$$

where $\varepsilon_t = \frac{\mathbf{x}(t) - a(t)\mathbf{x}(0)}{b(t)}$ and $\varepsilon_\theta(\mathbf{x}(t), t) = -b(t)\mathbf{s}_\theta(\mathbf{x}(t), t)$. The expectation over $p_{\text{data}}(\mathbf{x}(0))$ is approximated by an average over training data samples, whereas the expectation over $p(\mathbf{x}(t)|\mathbf{x}(0))$, which corresponds to simulating the forward process, is numerically performed by applying the perturbation kernel in Eq. (1) to $\mathbf{x}(0)$.

2.2 Improving the Sampling Efficiency

In addition to the distinction between training-free and -based methods, approaches for improving the sampling efficiency of diffusion models can be roughly categorized into one of two major branches:

Noise Scheduling Optimization: The two most popular noising schedules are variance-exploding (VE) [Song and Ermon, 2019, Song et al., 2021a] and variance-preserving (VP) [Ho et al., 2020] schedules. The original VE schedule uses $a(t) = 1$ and $b^2(t) = \sigma^2(t)$ to define the perturbation kernel in Eq. (1), and controls $\sigma(t)$, e.g., by setting $\sigma^2(t) = \sigma_{\min}^2 \left(\frac{\sigma_{\max}}{\sigma_{\min}} \right)^{2t}$, where σ_{\min} and σ_{\max} are the minimum and maximum noise level, respectively. In contrast, the VP schedule uses $a(t) = \sqrt{\bar{a}(t)}$ and $b^2(t) = 1 - a^2(t)$, and controls $\bar{a}(t)$, e.g., by $\bar{a}(t) = e^{-\beta_{\min} t - \frac{1}{2}(\beta_{\max} - \beta_{\min})t^2}$, where β_{\min} and β_{\max} control the start and end points of the schedule. Karras et al. [2022] introduced the EDM framework, which optimizes the reverse process to minimize the number of function evaluations (NFEs) while preserving sample quality. They design the noising schedule using a scale factor $s(t)$ and the noise level $\sigma(t)$, defined as:

$$p(\mathbf{x}(t)|\mathbf{x}(0)) = \mathcal{N}(\mathbf{x}(t); s(t)\mathbf{x}(0), s^2(t)\sigma^2(t)\mathbf{I}), \quad (6)$$

and adopt a non-uniform time grid discretization over N steps, $t_i = \sigma^{-1}(\sigma_i)$, where

$$\sigma_{i < N} = \left(\sigma_{\max}^{1/\rho} + \frac{i}{N-1} \left(\sigma_{\min}^{1/\rho} - \sigma_{\max}^{1/\rho} \right) \right)^\rho \quad (7)$$

and $\sigma_N = 0$ for $\rho = 7$. They argue that setting $s(t) = 1$ and $\sigma(t) = t$, which coincides with the DDIM sampler [Song et al., 2021b], leads to straight flow trajectories. Specifically, they argue that when $\lambda = 0$ in Eq. (4), this schedule minimizes the discretization error under some assumptions.

High-order Solvers and Distillation Approaches: Orthogonal to exploring optimized noise schedules, sampling efficiency can also be improved by adopting higher-order solvers, e.g., Heun’s method [Karras et al., 2022] or the DPM-solver [Lu et al., 2022b, Zheng et al., 2023], or by distillation approaches, such as consistency models [Song et al., 2023a, Lu and Song, 2025] and ReFlow [Kim et al., 2025], where an efficient yet highly non-linear (potentially one-shot) solver is trained by distilling diffusion models.

In this work, we focus on exploring optimal noise scheduling, and show that better schedules improve the performance across different choices of reverse diffusion solvers, which can be regarded as an orthogonal approach to improving diffusion models.

3 Proposed Methods

In this section, we first describe our unifying framework for noise scheduling, where the total variance (TV) and the signal-to-noise ratio (SNR) are controlled independently. Then, we cast established schedules into our framework, and apply simple modifications. We empirically show that, for common existing schedules where the TV grows exponentially, their constant TV (i.e., VP) variants consistently improve performance. Finally, we propose the ISSNR schedule, an SNR scheduling strategy based on the exponential of the inverse sigmoid function, further enhancing sampling efficiency and quality.

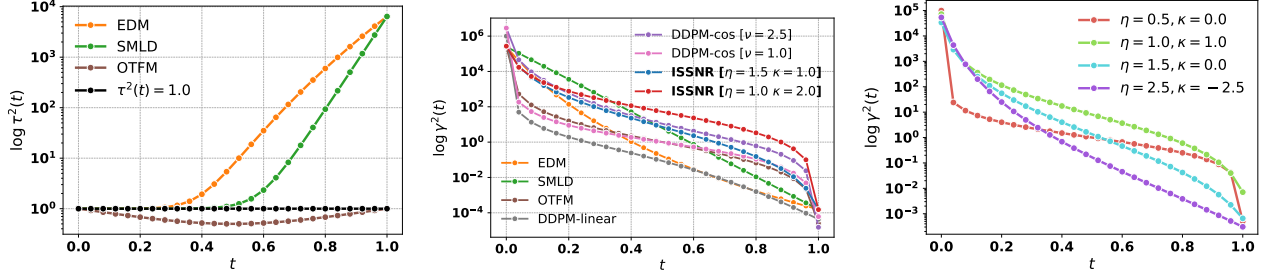


Figure 2: TV (left) and SNR (middle) schedules of different established scheduling methods (see Table A1 in Appendix A for the corresponding analytic expressions). Right: Our proposed inverse sigmoid SNR (ISSNR) schedule.

3.1 TV/SNR Disentangled Scheduling Framework

We reformulate the perturbation kernel in Eq. (1) as

$$p(\mathbf{x}(t)|\mathbf{x}(0)) = \mathcal{N} \left(\mathbf{x}(t); \sqrt{\frac{\tau^2(t)\gamma^2(t)}{1+\gamma^2(t)}} \mathbf{x}(0), \frac{\tau^2(t)}{1+\gamma^2(t)} \mathbf{I} \right), \quad (8)$$

where $\tau(\cdot) : [0, 1] \mapsto \mathbb{R}_{++}$ is a TV controlling function, and $\gamma(\cdot) : [0, 1] \mapsto \mathbb{R}_{++}$ is an SNR controlling function. $\tau(t)$ can be an arbitrary positive function, while $\gamma(t)$ is monotonically decreasing from $\gamma(0) = \gamma_{\max} < \infty$ to $\gamma(1) = \gamma_{\min} > 0$. By comparing Eq. (8) to Eq. (1), it is straightforward to confirm that

$$\text{TV} = a^2(t) + b^2(t) = \tau^2(t) \quad \text{and} \quad \text{SNR} = \frac{a(t)}{b(t)} = \gamma(t),$$

and therefore, $\tau(t)$ does not affect SNR and $\gamma(t)$ does not affect TV, respectively – they can be controlled independently. The forward and reverse SDEs corresponding to the kernel in Eq. (8) are given by Eqs. (3) and (4), respectively, with the drift and diffusion coefficients

$$f(t) = \frac{\dot{\tau}(t)}{\tau(t)} + \frac{\dot{\gamma}(t)}{\gamma(t)(1+\gamma^2(t))} \quad \text{and} \quad g(t) = \sqrt{\frac{-2\tau^2(t)\dot{\gamma}(t)}{\gamma(t)(1+\gamma^2(t))}}$$

(see Appendix B.3 for the full derivation). In practice, for numerical stability, we work in the logarithmic scale. Specifically, we use the identity $\frac{d}{dt} \log \gamma(t) = \frac{\dot{\gamma}(t)}{\gamma(t)}$, and apply the same transformation to $\tau(t)$.

3.2 VP Variants of Established Non-VP Schedules

For common established schedules, including the original linear VP schedule in DDPM [Ho et al., 2020, Song et al., 2021a] and its cosine alternative [Nichol and Dhariwal, 2021], the original VE schedule in SMLD [Song and Ermon, 2019, Song et al., 2021a], EDM [Karras et al., 2022], and FM [Lipman et al., 2023], Figure 2 (left and middle) show their corresponding TV and SNR schedules (see Appendix A for derivations, as well as Table A1 for analytic expressions). Since EDM uses a non-uniform time grid, we also consider EDM with a uniform time grid (EDM-UT), where we incorporate the original non-uniform time grid into the TV/SNR schedules. Note that, although EDM and EDM-UT effectively use the same schedules and their respective ODEs are equivalent in the continuous time case, they perform differently when using numerical integration with discretization to solve the ODE/SDE. SMLD, EDM, and EDM-UT all use a VE schedule, where the TV increases exponentially to a large value σ_{\max} when $t \rightarrow 1$. The TV schedule of the optimal transport flow matching (OTFM) is modulated, i.e., it is a variance-modulated (VM) schedule, although it does not grow exponentially, as depicted in Figure 2 (left). In Section 4, we examine whether exploding or modulated TV schedules are essential for achieving good performance. To this end, we introduce their VP counterparts, VP-SMLD, VP-EDM-UT, and VP-OTFM, which use a constant TV schedule and the original SNR schedules (see Table A1).

3.3 Variance-preserving Inverse Sigmoid SNR (VP-ISSNR) Schedule

We propose to schedule TV and SNR with the following functions:

$$\tau^2(t) = 1, \quad (9)$$

$$\gamma^2(t) = \exp \left(2\eta \log \left(\frac{1}{t(t_{\max} - t_{\min}) + t_{\min}} - 1 \right) + 2\kappa \right) = \left(\frac{1}{t(t_{\max} - t_{\min}) + t_{\min}} - 1 \right)^{2\eta} \exp(2\kappa). \quad (10)$$

Namely, we set TV to be constant, and schedule SNR with the exponential of the inverse sigmoid function. The parameters $\eta > 0$ and $\kappa \in \mathbb{R}$ control the steepness and the offset of the inverse sigmoid function, respectively, and the two constants $0 < t_{\min} \approx 0$ and $1 > t_{\max} \approx 1$ adjust the starting γ_{\max} and final γ_{\min} SNR values as

$$\gamma^2(0) = \exp\left(2\eta \log\left(\frac{1}{t_{\min}} - 1\right) + 2\kappa\right) = \gamma_{\max}^2, \quad (11)$$

$$\gamma^2(1) = \exp\left(2\eta \log\left(\frac{1}{t_{\max}} - 1\right) + 2\kappa\right) = \gamma_{\min}^2. \quad (12)$$

The right panel in Figure 2 shows the inverse sigmoid function from Eq. (10) with different parameter choices. With this SNR function, we can allocate more steps to specific SNR levels using κ , while η controls the relative emphasis on the most critical SNR levels compared to other regions of the diffusion process.

Relation to OTFM Using optimal transport (OT) to define the conditional probability path in flow matching (FM) [Lipman et al., 2023] results in a linear interpolation between the prior and the target data distribution,

$$p_t(\mathbf{x}_t | \mathbf{x}_0) = \mathcal{N}(\mathbf{x}(t); (1-t)\mathbf{x}(0), ((1-t)\sigma_{\min} + t)^2 \mathbf{I}), \quad (13)$$

where σ_{\min} is chosen to be sufficiently small, ensuring that the Gaussian distribution is concentrated around the target data point $x(0)$.² Consider a generalization of Eq. (13):

$$p_t(\mathbf{x}_t | \mathbf{x}_0) = \mathcal{N}(\mathbf{x}(t); (1-t)^{\eta} \mathbf{x}(0), t^{2\eta} \exp(-2\kappa) \mathbf{I}). \quad (14)$$

Then, the corresponding TV and SNR schedules are

$$\tau^2(t) = (1-t)^{2\eta} + t^{2\eta} \exp(-2\kappa) \quad \text{and} \quad \gamma^2(t) = \left(\frac{1}{t} - 1\right)^{2\eta} \exp(2\kappa).$$

Comparing these expressions to our proposed ISSNR schedules in Eqs. (9) and (10), we observe that our proposed SNR schedule is a generalization of the OTFM in Eq. (14) with a constant TV schedule (setting $\eta = 1.0$ and $\kappa = 0$ recovers the SNR schedule of OTFM). The generalization allows for more control over the generated probability flow.

4 Experiments

In this section, we empirically evaluate our proposed TV/SNR scheduling framework on molecular structure and image generation tasks. We also discuss the conditions for good schedules in terms of the paths of ODE trajectories and the time evolution of the marginal density through toy numerical investigations.

4.1 Molecular Structure Generation

Problem setting: The goal is to predict an equilibrium state R given a molecular composition Z , i.e., $\mathbf{x}(0) \sim p(R|Z)$. Note the difference from the general molecule generation task, where the composition Z is also predicted. Our experiments systematically evaluate different scheduling techniques used in SOTA diffusion and flow matching models for molecular tasks [Hoogeboom et al., 2022, Xu et al., 2023, Vignac et al., 2023, Kahouli et al., 2024, Song et al., 2023b, Le et al., 2024, Hassan et al., 2024]. Common schedules include DDPM-cos with $\nu = 1$ and $\nu = 2.5$ and OTFM. We use the QM9 dataset [Ramakrishnan et al., 2014], a widely used benchmark comprising $\sim 130k$ equilibrium molecules with up to 9 heavy atoms (C, O, N, and F) for our evaluation. Following Kahouli et al. [2024], we use a training/validation split of 55k/10k molecules and the remainder for testing. For training, we adopt the noise model architecture used in Kahouli et al. [2024] and minimize the DSM loss (5) using the DDPM-cos schedule with $\nu = 1.0$. Unless otherwise stated, for sample generation, we solve the reverse ODE in Eq. (4) for $\lambda = 0$, using first-order Euler integration. For varying computational budgets, defined by the number of function evaluations (NFEs), we report stability rates [Gebauer et al., 2022] (higher is better) over 2.5k generated structures with compositions Z sampled from the test split. More experimental details are given in Appendix C.

VP-variants of Existing Schedules: Figure 3 (left) presents a comparison of the stability rates of VE schedules, SMLD and EDM-UT, as well as the VM schedule OTFM, against their VP counterparts: VP-SMLD, VP-EDM-UT, and VP-OTFM. Importantly, across all schedules, the VP variants outperform or match the performance of their original versions. Specifically, the VP versions lead to substantial enhancements for SMLD and EDM-UT, where the TV increases exponentially, whereas OTFM with a smooth TV modulation performs comparably to its VP analog. These findings suggest that exponentially increasing TV can be detrimental, thereby validating our choice to adopt a constant TV schedule.

²Note that in Lipman et al. [2023], the time is reversed, with $\mathbf{x}(1)$ and $\mathbf{x}(0)$ corresponding to the samples in the target and latent domain, respectively. In this paper, we always define t in the forward diffusion direction.

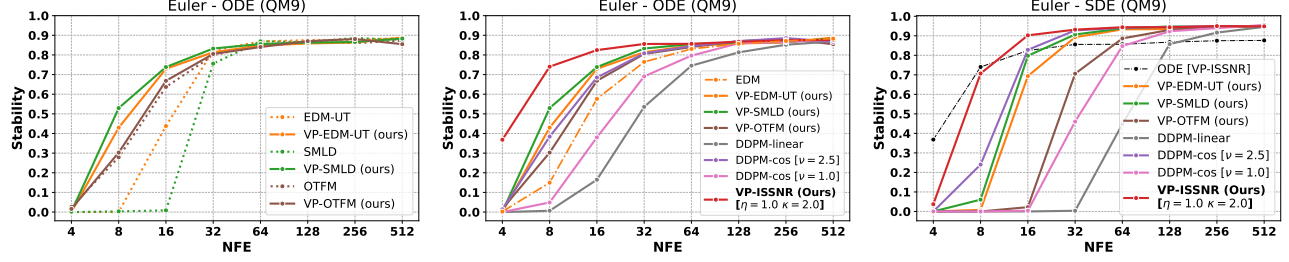


Figure 3: Stability rate (**higher is better**) as a function of the number of function evaluations (NFE) for molecular structure generation on the QM9 dataset. Left: Comparison between commonly established non-VP schedules (i.e., $\tau(t)$ non-constant) and their VP counterparts in our framework. Middle: Comparison of various baselines, including the VP analogs from the left plot, against our proposed VP-ISSNR schedule, with fixed parameters $\eta = 1.0$ and $\kappa = 2.0$ for all NFEs. Right: Same as the middle plot but using the reverse SDE, instead of the reverse ODE. The best-performing ODE schedule, VP-ISSNR, is highlighted in black for reference.

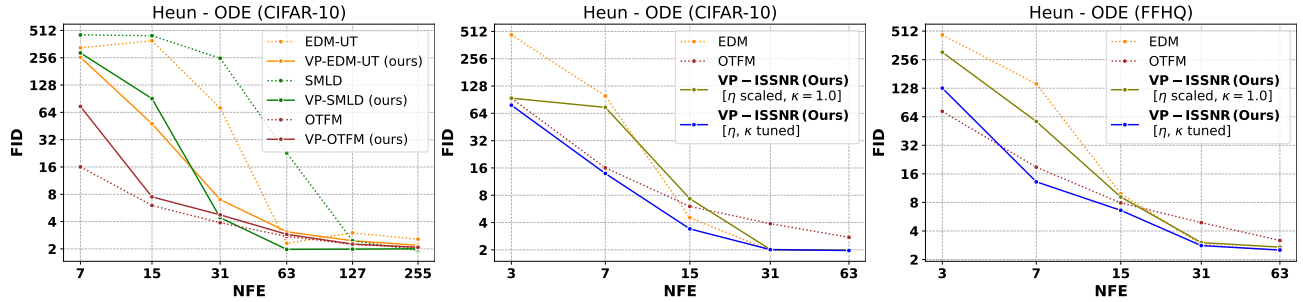


Figure 4: FID score (**lower is better**) as a function of the number of function evaluations (NFE) for image generation on CIFAR-10 and FFHQ. Left: Comparison of existing non-VP models and their VP variants on CIFAR-10. Middle: Comparison on CIFAR-10 between baseline methods and two variants of our proposed VP-ISSNR method, one using a scaled η in function of the NFE, and the other tuning η and κ for each NFE via Bayesian optimization, as detailed in Section 4.2. Right: Same comparison as in the middle, but on higher-resolution FFHQ images.

VP-ISSNR Schedule: Figure 3 (middle) presents results for all methods shown in Figure 2, excluding the original VE schedules, which perform worse compared to their VP analogs (shown in the left plot). It also includes the original OTFM and EDM (with non-uniform time grid) and our proposed VP-ISSNR schedule, using the fixed parameters $\eta = 1.0$, $\kappa = 2.0$, $t_{\min} = 0.01$ and $t_{\max} = 0.99$ for all NFE values. Strikingly, the diffusion model generates stable molecules in as few as 4 NFEs with a first-order solver when using our VP-ISSNR schedule. The stability rate surpasses 74% with only 8 steps and reaches nearly 87% with 128 steps, outperforming all other schedules. Additionally, Figure 3 (right) shows that, when solving the reverse SDE ($\lambda = 1$ in Eq.(4)) using our VP-ISSNR schedule, the stability rate increases significantly to 93.16% with 32 NFEs and 95.82% with 64 NFEs. To the best of our knowledge, these results are SOTA for the given NFEs. While the ODE achieves a higher stability rate than the SDE at very low NFEs (e.g., 74% vs. 70% at 8 NFEs), the SDE achieves superior stability as NFEs increase, suggesting that stochasticity introduces a corrective effect that enhances sample quality in molecules, albeit with a slight increase in sampling time. In Figure A2 in Appendix D.1, we present additional experimental results using the second-order Heun’s method and the advanced DPM solver [Lu et al., 2022a, 2023], where we observe similar trends. This demonstrates that our noise schedule optimization is *orthogonal* to the choice of sampler, i.e., it can be combined with advanced sampling methods for even larger overall improvements. We also report the results of training models with different schedules in Figure A4, and assess the quality of samples by running DFT relaxations to identify the nearest reference structure in Figure A3, mirroring the trends in the stability rate results.

4.2 Image Generation

Problem setting: We evaluate the performance of different schedules for unconditional image generation. Following the setup in Karras et al. [2022], we use their pre-trained diffusion models and assess sample quality using the average FID score [Heusel et al., 2017] computed over 50k generated images as a function of NFEs on CIFAR-10 [Krizhevsky, 2009] and the higher-resolution FFHQ [Karras et al., 2018]. Unless otherwise stated, samples are generated by solving the reverse ODE using the commonly used second-order Heun’s method.

VP-variants of Existing Schedules: Similar to the experiment with molecules in Figure 3 (left), we first compare the original non-VP schedules to their VP analogs. Figure 4 (left) summarizes the performance on CIFAR-10 (results on FFHQ show similar trends, see Appendix D). Consistent with our findings for molecular structure generation, we observe that both SMLD and EDM-UT, which feature exploding TV schedules, benefit significantly from adopting a constant TV schedule. In contrast, the VP-OTFM does not perform as well as the original OTFM with modulated TV, which is different from what we observe for molecular structure generation. This implies the possibility of further improving fast sampling by optimizing the TV control, which we leave as future work.

VP-ISSNR Schedule: Figure 4 (middle) and Figure 4 (right) compare different schedules, including the original EDM, OTFM and our proposed VP-ISSNR schedule. Unlike in molecular structure generation, the original EDM outperforms other methods in image generation. This is somewhat expected, as EDM is highly optimized for this task. Its strong performance relies on a carefully tuned non-uniform time grid, as evidenced by the poor results of its uniform-time variant (EDM-UT) in Figure 4 (left). Our proposed inverse sigmoid (ISSNR) schedule has two free hyperparameters η and κ . While fixing these to constant values is sufficient to achieve SOTA performance for molecule generation, this is not the case for images. We therefore explore a simple modification ISSNR [scaled], where we scale η logarithmically as $\eta = 2 + \max(0, \log_2(nfe + 1) - 3)$ with the NFEs and set $\kappa = 0$. This schedule achieves competitive results across all image datasets, as illustrated in the middle and right panels in Figure 4. To further enhance performance, it is possible to tune η and κ for different datasets and NFEs (we use Bayesian optimization over 32 trials to find optimized values). We refer to this variant as ISSNR [tuned]. For completeness, additional experiments with results for fixed values of η and κ are presented in Appendix D.2. With optimally tuned hyperparameters, our ISSNR yields improved image quality in terms of FID, particularly in the low-NFE regime. To evaluate the generalizability and orthogonality of our approach to different choices of solvers, we also assess its performance using the first-order Euler, the higher-order Runge–Kutta (RK45), and the advanced DPM solvers [Lu et al., 2022a, 2023]. Results are reported in Figure A6 in Appendix D.2, showing consistent trends across solvers. Additionally, we include results on more high-resolution datasets such as AFHQ [Choi et al., 2020] and ImageNet [Deng et al., 2009] in Figure A7.

To summarize the results, our TV/SNR framework is robust and effective across domains, as evidenced by its strong performance in both molecular structure and image generation tasks. Moreover, we observe consistent quality improvements across different solvers, suggesting that our scheduling approach is *orthogonal* to other methods that make sampling of diffusion models more efficient.

4.3 Discussion: Curvature of ODE Trajectories and the Support of Marginal Density

Karras et al. [2022] argue that, if ODE trajectories follow straight paths, crude time discretization should not produce substantial errors, enabling fast sample generation. They further argue from a theoretical point of view that ODE trajectories of EDM are straight, by using Tweedie’s formula [Efron, 2011], $\nabla_x \log p_t(\mathbf{x}(t)) = \frac{a(t)\mathbb{E}[\mathbf{x}(0)|\mathbf{x}(t)] - \mathbf{x}(t)}{b^2(t)}$. However, this argument assumes that the conditional expectation $\mathbb{E}[\mathbf{x}(0)|\mathbf{x}(t)]$ approximates the data point $\mathbf{x}(0)$ that $\mathbf{x}(t)$ reaches at time $t = 0$ in the reverse ODE process, which does not necessarily hold due to the *interaction between trajectories* – an ODE trajectory generating a particular data point never crosses the trajectory of another data point. To demonstrate such trajectory interactions, Figure 1B depicts ODE trajectories of EDM, OTFM, and our VP-ISSNR for a toy problem where the data distribution $p_{\text{data}}(\mathbf{x}(0))$ is a mixture of three delta peaks with equal weights (uniformly spaced at $x = 0, \pm\sqrt{3/2}$, such that the mean and variance are standardized). The ODE trajectories are obtained by solving the reverse ODE with the exact score function, which can be computed analytically in this case. At first glance, the trajectories of EDM (top) seem straight, however, focusing on the neighborhood of a single delta peak (e.g., $x = \sqrt{3/2}$) close to the data space ($t \rightarrow 0$), reveals that trajectories are highly curved (see inset). Quantifying the local curvature along trajectories as $\mathbb{E}[\|(\mathbf{x}(1) - \mathbf{x}(0)) - \dot{\mathbf{x}}(t)\|^2]$ [Liu et al., 2023b] (see green curves in Figure 1B) shows that our VP-ISSNR schedule leads to trajectories with smaller curvature than both EDM and OTFM. Here $\dot{\mathbf{x}}(t)$ represents the time derivative of $\mathbf{x}(t)$, and the overall/global curvature across the whole trajectory can be obtained by integrating over t . For completeness, Figure A8 in Appendix D.3 shows ODE trajectories for all schedules in Section 4.

We hypothesize that discretization errors around $t \approx 0$ are more severe than errors around $t \approx 1$, because errors arising when the marginal $p_t(\mathbf{x})$ has large support (due to the Gaussian diffusion) should not strongly affect sample quality at $t = 0$. This is because such errors do not push the latent sample $\mathbf{x}(t)$ into the out-of-distribution region of $p_t(\mathbf{x})$. Instead, they steer samples onto an “incorrect” trajectory, potentially violating bijectiveness. However, if the remaining reverse process is solved accurately, samples following such incorrect trajectories can still reach high-quality points at $t = 0$. Thus, we hypothesize that a good schedule should i) have straight trajectories close to the data space ($t \approx 0$), and ii) the support of the marginal density $p_t(\mathbf{x})$ (relative to the variance at $t = 1$) should grow quickly, ideally saturating before t reaches 1. We observe that for schedules with exploding TV, e.g., SMLD and EDM-UT, the support of the marginal $p_t(\mathbf{x})$ steadily increases until $t = 1$ (see Figure A8). In contrast, schedules with non-exploding $\tau(t)$, like OTFM and VP schedules, already reach (close to) maximum

support for $t < 1$. The relative support $b(t)/b(t_{\max})$ of the marginal distributions is quantified in Figures 1B and A8 (see red curves), which numerically confirms these trends. Trajectories sampled with our VP-ISSNR schedule have low overall curvature, while the local curvature is only high in regions with large support. Thus, our hypothesis would explain why the VP-ISSNR schedule and VP variants of existing VE schedules improve sample quality. Further, we find that OTFM, our VP-OTFM, and our VP-ISSNR lead to straight trajectories around $t \approx 0$, which is consistent with our experimental results on molecule and image generation. The reason why EDM performs so well for image generation despite the high curvature of trajectories around $t \approx 0$ is likely because the non-uniform time grid assigns most integration steps precisely in this region (indicated by the density of ticks on the x -axis in Figures 1B, A8, and A1 in Appendix A), which mitigates discretization errors.

5 Conclusion

The performance and sampling efficiency of diffusion models are highly dependent on the chosen noise schedules, which manage the trade-off between noise injection and signal preservation. Existing schedules often control variance implicitly, lacking direct control over this crucial balance.

In this work, we propose a novel total-variance/signal-to-noise-ratio disentangled (TV/SNR) framework for designing noise schedules, which allows controlling TV and SNR *independently*. We empirically find that existing schedules where the TV grows exponentially can be *improved* by instead keeping TV constant while leaving the SNR schedule unchanged. Our TV/SNR framework enables the design of noise schedules that perform on par with the highly optimized EDM sampler for image generation, and lead to clear performance improvements when generating molecules. Specifically, we propose the ISSNR schedule as a generalization of optimal transport flow matching, and find that it leads to drastic performance improvements (up to 30-fold) in molecular structure generation: Stable molecules can be generated after only 4 steps (much less than the previous SOTA). By further tuning the hyperparameters of the ISSNR schedule, it is even possible to improve upon the EDM sampler for image generation. To obtain further insights into these empirical findings, we analyze ODE trajectories for a simple toy model and hypothesize which mechanisms are responsible for the observed increased sample efficiency.

In conclusion, reformulating diffusion processes within our TV/SNR framework enables a new way to improve the efficiency of diffusion models, leading to significant progress in domains like molecular structure generation.

Acknowledgments

This work was partly funded by the German Ministry for Education and Research (BMBF) as BIFOLD – Berlin Institute for the Foundations of Learning and Data - under Grants 01IS14013A-E, 01GQ1115, 01GQ0850, 01IS18025A, 031L0207D, and 01IS18037A. Furthermore, K.R.M. was partly supported by the Institute of Information & Communications Technology Planning & Evaluation (IITP) grants funded by the Korean Government (MSIT) (No. 2019-0-00079, Artificial Intelligence Graduate School Program, Korea University and No. 2022-0-00984, Development of Artificial Intelligence Technology for Personalized Plug-and-Play Explanation and Verification of Explanation). S.G. was supported by the Postdoc.Mobility fellowship by the Swiss National Science Foundation (project no. 225476).

References

Jascha Sohl-Dickstein, Eric Weiss, Niru Maheswaranathan, and Surya Ganguli. Deep unsupervised learning using nonequilibrium thermodynamics. In Francis Bach and David Blei, editors, *Proceedings of the 32nd International Conference on Machine Learning*, volume 37 of *Proceedings of Machine Learning Research*, pages 2256–2265, Lille, France, 07–09 Jul 2015. PMLR. URL <https://proceedings.mlr.press/v37/sohl-dickstein15.html>.

Jonathan Ho, Ajay Jain, and Pieter Abbeel. Denoising diffusion probabilistic models. In H. Larochelle, M. Ranzato, R. Hadsell, M.F. Balcan, and H. Lin, editors, *Advances in Neural Information Processing Systems*, volume 33, pages 6840–6851. Curran Associates, Inc., 2020. URL https://proceedings.neurips.cc/paper_files/paper/2020/file/4c5bcfec8584af0d967f1ab10179ca4b-Paper.pdf.

Yang Song and Stefano Ermon. Improved techniques for training score-based generative models. In H. Larochelle, M. Ranzato, R. Hadsell, M.F. Balcan, and H. Lin, editors, *Advances in Neural Information Processing Systems*, volume 33, pages 12438–12448. Curran Associates, Inc., 2020. URL https://proceedings.neurips.cc/paper_files/paper/2020/file/92c3b916311a5517d9290576e3ea37ad-Paper.pdf.

Yang Song, Jascha Sohl-Dickstein, Diederik P Kingma, Abhishek Kumar, Stefano Ermon, and Ben Poole. Score-based generative modeling through stochastic differential equations. In *International Conference on Learning Representations*, 2021a. URL <https://openreview.net/forum?id=PxTIG12RRHS>.

Prafulla Dhariwal and Alexander Quinn Nichol. Diffusion models beat GANs on image synthesis. In A. Beygelzimer, Y. Dauphin, P. Liang, and J. Wortman Vaughan, editors, *Advances in Neural Information Processing Systems*, 2021. URL <https://openreview.net/forum?id=AAWuCvzaVt>.

Alexander Quinn Nichol, Prafulla Dhariwal, Aditya Ramesh, Pranav Shyam, Pamela Mishkin, Bob McGrew, Ilya Sutskever, and Mark Chen. GLIDE: Towards photorealistic image generation and editing with text-guided diffusion models. In Kamalika Chaudhuri, Stefanie Jegelka, Le Song, Csaba Szepesvari, Gang Niu, and Sivan Sabato, editors, *Proceedings of the 39th International Conference on Machine Learning*, volume 162 of *Proceedings of Machine Learning Research*, pages 16784–16804. PMLR, 17–23 Jul 2022. URL <https://proceedings.mlr.press/v162/nichol22a.html>.

Robin Rombach, Andreas Blattmann, Dominik Lorenz, Patrick Esser, and Björn Ommer. High-resolution image synthesis with latent diffusion models. In *Proceedings of the IEEE/CVF conference on computer vision and pattern recognition (CVPR)*, pages 10684–10695, 2022.

William Peebles and Saining Xie. Scalable diffusion models with transformers. In *Proceedings of the IEEE/CVF International Conference on Computer Vision (ICCV)*, pages 4195–4205, October 2023.

Nanye Ma, Mark Goldstein, Michael S. Albergo, Nicholas M. Boffi, Eric Vanden-Eijnden, and Saining Xie. Sit: Exploring flow and diffusion-based generative models with scalable interpolant transformers. In Aleš Leonardis, Elisa Ricci, Stefan Roth, Olga Russakovsky, Torsten Sattler, and Gülcin Varol, editors, *Computer Vision – ECCV 2024*, pages 23–40, Cham, 2024. Springer Nature Switzerland.

Zhifeng Kong, Wei Ping, Jiaji Huang, Kexin Zhao, and Bryan Catanzaro. Diffwave: A versatile diffusion model for audio synthesis. In *International Conference on Learning Representations*, 2021. URL <https://openreview.net/forum?id=a-xFK8Ymz5J>.

Nanxin Chen, Yu Zhang, Heiga Zen, Ron J Weiss, Mohammad Norouzi, and William Chan. Wavegrad: Estimating gradients for waveform generation. In *International Conference on Learning Representations*, 2021. URL <https://openreview.net/forum?id=NsMLjcFa080>.

Haohe Liu, Zehua Chen, Yi Yuan, Xinhao Mei, Xubo Liu, Danilo Mandic, Wenwu Wang, and Mark D Plumbley. AudioLDM: Text-to-audio generation with latent diffusion models. In Andreas Krause, Emma Brunskill, Kyunghyun Cho, Barbara Engelhardt, Sivan Sabato, and Jonathan Scarlett, editors, *Proceedings of the 40th International Conference on Machine Learning*, volume 202 of *Proceedings of Machine Learning Research*, pages 21450–21474. PMLR, 23–29 Jul 2023a. URL <https://proceedings.mlr.press/v202/liu23f.html>.

Niklas WA Gebauer, Michael Gastegger, Stefaan SP Hessmann, Klaus-Robert Müller, and Kristof T Schütt. Inverse design of 3d molecular structures with conditional generative neural networks. *Nature communications*, 13:973, 2022.

Emiel Hoogeboom, Víctor Garcia Satorras, Clément Vignac, and Max Welling. Equivariant diffusion for molecule generation in 3D. In Kamalika Chaudhuri, Stefanie Jegelka, Le Song, Csaba Szepesvari, Gang Niu, and Sivan Sabato, editors, *Proceedings of the 39th International Conference on Machine Learning*, volume 162 of *Proceedings of Machine Learning Research*, pages 8867–8887. PMLR, 17–23 Jul 2022. URL <https://proceedings.mlr.press/v162/hoogeboom22a.html>.

Lemeng Wu, Chengyue Gong, Xingchao Liu, Mao Ye, and Qiang Liu. Diffusion-based molecule generation with informative prior bridges. In S. Koyejo, S. Mohamed, A. Agarwal, D. Belgrave, K. Cho, and A. Oh, editors, *Advances in Neural Information Processing Systems*, volume 35, pages 36533–36545. Curran Associates, Inc., 2022.

Lei Huang, Hengtong Zhang, Tingyang Xu, and Ka-Chun Wong. Mdm: Molecular diffusion model for 3d molecule generation. *Proceedings of the AAAI Conference on Artificial Intelligence*, 37(4):5105–5112, Jun. 2023. doi:10.1609/aaai.v37i4.25639. URL <https://ojs.aaai.org/index.php/AAAI/article/view/25639>.

Minkai Xu, Alexander S Powers, Ron O. Dror, Stefano Ermon, and Jure Leskovec. Geometric latent diffusion models for 3D molecule generation. In Andreas Krause, Emma Brunskill, Kyunghyun Cho, Barbara Engelhardt, Sivan Sabato, and Jonathan Scarlett, editors, *Proceedings of the 40th International Conference on Machine Learning*, volume 202 of *Proceedings of Machine Learning Research*, pages 38592–38610. PMLR, 23–29 Jul 2023. URL <https://proceedings.mlr.press/v202/xu23n.html>.

Xingang Peng, Jiaqi Guan, Qiang Liu, and Jianzhu Ma. MolDiff: Addressing the atom-bond inconsistency problem in 3D molecule diffusion generation. In Andreas Krause, Emma Brunskill, Kyunghyun Cho, Barbara Engelhardt, Sivan Sabato, and Jonathan Scarlett, editors, *Proceedings of the 40th International Conference on Machine Learning*, volume 202 of *Proceedings of Machine Learning Research*, pages 27611–27629. PMLR, 23–29 Jul 2023. URL <https://proceedings.mlr.press/v202/peng23b.html>.

Clement Vignac, Nagham Osman, Laura Toni, and Pascal Frossard. Midi: Mixed graph and 3d denoising diffusion for molecule generation. In *ICLR 2023 - Machine Learning for Drug Discovery workshop*, 2023. URL <https://openreview.net/forum?id=M6Ifac3G4HK>.

Tuan Le, Julian Cremer, Frank Noe, Djork-Arné Clevert, and Kristof T Schütt. Navigating the design space of equivariant diffusion-based generative models for de novo 3d molecule generation. In *The Twelfth International Conference on Learning Representations*, 2024. URL <https://openreview.net/forum?id=kzGuiRXZrQ>.

Khaled Kahouli, Stefaan Simon Pierre Hessmann, Klaus-Robert Müller, Shinichi Nakajima, Stefan Gugler, and Niklas Wolf Andreas Gebauer. Molecular relaxation by reverse diffusion with time step prediction. *Machine Learning: Science and Technology*, 5(3):035038, aug 2024. doi:10.1088/2632-2153/ad652c. URL <https://dx.doi.org/10.1088/2632-2153/ad652c>.

Minkai Xu, Lantao Yu, Yang Song, Chence Shi, Stefano Ermon, and Jian Tang. GeoDiff: A geometric diffusion model for molecular conformation generation. In *International Conference on Learning Representations*, 2022. URL <https://openreview.net/forum?id=PzcvxEMzvQC>.

Alexander Quinn Nichol and Prafulla Dhariwal. Improved denoising diffusion probabilistic models. In Marina Meila and Tong Zhang, editors, *Proceedings of the 38th International Conference on Machine Learning*, volume 139 of *Proceedings of Machine Learning Research*, pages 8162–8171. PMLR, 18–24 Jul 2021. URL <https://proceedings.mlr.press/v139/nichol21a.html>.

Daniel Watson, William Chan, Jonathan Ho, and Mohammad Norouzi. Learning fast samplers for diffusion models by differentiating through sample quality. In *International Conference on Learning Representations*, 2022. URL <https://openreview.net/forum?id=VFBjuF8HEp>.

Tim Salimans and Jonathan Ho. Progressive distillation for fast sampling of diffusion models. In *International Conference on Learning Representations*, 2022. URL <https://openreview.net/forum?id=TIdIXIpzhoI>.

Yang Song, Prafulla Dhariwal, Mark Chen, and Ilya Sutskever. Consistency models. In Andreas Krause, Emma Brunskill, Kyunghyun Cho, Barbara Engelhardt, Sivan Sabato, and Jonathan Scarlett, editors, *Proceedings of the 40th International Conference on Machine Learning*, volume 202 of *Proceedings of Machine Learning Research*, pages 32211–32252. PMLR, 23–29 Jul 2023a. URL <https://proceedings.mlr.press/v202/song23a.html>.

Cheng Lu and Yang Song. Simplifying, stabilizing and scaling continuous-time consistency models. In *The Thirteenth International Conference on Learning Representations*, 2025. URL <https://openreview.net/forum?id=LyJi5ugyJx>.

Beomsu Kim, Yu-Guan Hsieh, Michal Klein, marco cuturi, Jong Chul Ye, Bahjat Kawar, and James Thornton. Simple reflow: Improved techniques for fast flow models. In *The Thirteenth International Conference on Learning Representations*, 2025. URL <https://openreview.net/forum?id=fPvgSDKXGY>.

Cheng Lu, Yuhao Zhou, Fan Bao, Jianfei Chen, Chongxuan Li, and Jun Zhu. DPM-solver: A fast ODE solver for diffusion probabilistic model sampling in around 10 steps. In Alice H. Oh, Alekh Agarwal, Danielle Belgrave, and Kyunghyun Cho, editors, *Advances in Neural Information Processing Systems*, 2022a. URL https://openreview.net/forum?id=2uAaGw1P_V.

Luping Liu, Yi Ren, Zhipie Lin, and Zhou Zhao. Pseudo numerical methods for diffusion models on manifolds. In *International Conference on Learning Representations*, 2022. URL <https://openreview.net/forum?id=PlKWWd2yBky>.

Tim Dockhorn, Arash Vahdat, and Karsten Kreis. GENIE: Higher-order denoising diffusion solvers. In Alice H. Oh, Alekh Agarwal, Danielle Belgrave, and Kyunghyun Cho, editors, *Advances in Neural Information Processing Systems*, 2022. URL <https://openreview.net/forum?id=LKEYuYNOqx>.

Alexia Jolicoeur-Martineau, Ke Li, Rémi Piché-Taillefer, Tal Kachman, and Ioannis Mitliagkas. Gotta go fast when generating data with score-based models, 2022. URL <https://openreview.net/forum?id=YmONQIWli-->.

Kaiwen Zheng, Cheng Lu, Jianfei Chen, and Jun Zhu. DPM-solver-v3: Improved diffusion ODE solver with empirical model statistics. In *Thirty-seventh Conference on Neural Information Processing Systems*, 2023. URL <https://openreview.net/forum?id=9fWKExmKa0>.

Qinsheng Zhang and Yongxin Chen. Fast sampling of diffusion models with exponential integrator. In *The Eleventh International Conference on Learning Representations*, 2023. URL <https://openreview.net/forum?id=Loek7hfb46P>.

Wenliang Zhao, Lujia Bai, Yongming Rao, Jie Zhou, and Jiwen Lu. UniPC: A unified predictor-corrector framework for fast sampling of diffusion models. In *Thirty-seventh Conference on Neural Information Processing Systems*, 2023. URL <https://openreview.net/forum?id=hrkmlPhp1u>.

Ting Chen. On the importance of noise scheduling for diffusion models. *arXiv preprint arXiv:2301.10972*, 2023.

Shanchuan Lin, Bingchen Liu, Jiashi Li, and Xiao Yang. Common diffusion noise schedules and sample steps are flawed. In *Proceedings of the IEEE/CVF winter conference on applications of computer vision*, pages 5404–5411, 2024.

Tero Karras, Miika Aittala, Timo Aila, and Samuli Laine. Elucidating the design space of diffusion-based generative models. In Alice H. Oh, Alekh Agarwal, Danielle Belgrave, and Kyunghyun Cho, editors, *Advances in Neural Information Processing Systems*, 2022. URL <https://openreview.net/forum?id=k7FuT0WM0c7>.

Xingchao Liu, Chengyue Gong, and qiang liu. Flow straight and fast: Learning to generate and transfer data with rectified flow. In *The Eleventh International Conference on Learning Representations*, 2023b. URL <https://openreview.net/forum?id=XVjTT1nw5z>.

Yaron Lipman, Ricky T. Q. Chen, Heli Ben-Hamu, Maximilian Nickel, and Matthew Le. Flow matching for generative modeling. In *The Eleventh International Conference on Learning Representations*, 2023. URL <https://openreview.net/forum?id=PqvMRDCJT9t>.

Michael Samuel Albergo and Eric Vanden-Eijnden. Building normalizing flows with stochastic interpolants. In *The Eleventh International Conference on Learning Representations*, 2023. URL <https://openreview.net/forum?id=li7qeBbCR1t>.

Aram-Alexandre Pooladian, Heli Ben-Hamu, Carles Domingo-Enrich, Brandon Amos, Yaron Lipman, and Ricky T. Q. Chen. Multisample flow matching: Straightening flows with minibatch couplings. In Andreas Krause, Emma Brunskill, Kyunghyun Cho, Barbara Engelhardt, Sivan Sabato, and Jonathan Scarlett, editors, *Proceedings of the 40th International Conference on Machine Learning*, volume 202 of *Proceedings of Machine Learning Research*, pages 28100–28127. PMLR, 23–29 Jul 2023. URL <https://proceedings.mlr.press/v202/pooladian23a.html>.

Alexander Tong, Kilian FATRAS, Nikolay Malkin, Guillaume Huguet, Yanlei Zhang, Jarrid Rector-Brooks, Guy Wolf, and Yoshua Bengio. Improving and generalizing flow-based generative models with minibatch optimal transport. *Transactions on Machine Learning Research*, 2024. ISSN 2835-8856. URL <https://openreview.net/forum?id=CD9Snc73AW>. Expert Certification.

Leon Klein, Andreas Krämer, and Frank Noe. Equivariant flow matching. In *Thirty-seventh Conference on Neural Information Processing Systems*, 2023. URL <https://openreview.net/forum?id=eLH2NF001B>.

Yuxuan Song, Jingjing Gong, Minkai Xu, Ziyao Cao, Yanyan Lan, Stefano Ermon, Hao Zhou, and Wei-Ying Ma. Equivariant flow matching with hybrid probability transport for 3d molecule generation. In *Thirty-seventh Conference on Neural Information Processing Systems*, 2023b. URL <https://openreview.net/forum?id=hHUZ5V9XFu>.

Ross Irwin, Alessandro Tibo, Jon Paul Janet, and Simon Olsson. Efficient 3d molecular generation with flow matching and scale optimal transport. In *ICML 2024 AI for Science Workshop*, 2024. URL <https://openreview.net/forum?id=CxAjGjdkqu>.

Yang Song and Stefano Ermon. Generative modeling by estimating gradients of the data distribution. In H. Wallach, H. Larochelle, A. Beygelzimer, F. d’Alché-Buc, E. Fox, and R. Garnett, editors, *Advances in Neural Information Processing Systems*, volume 32. Curran Associates, Inc., 2019. URL https://proceedings.neurips.cc/paper_files/paper/2019/file/3001ef257407d5a371a96cd947c7d93-Paper.pdf.

Diederik P Kingma, Tim Salimans, Ben Poole, and Jonathan Ho. Variational diffusion models. In A. Beygelzimer, Y. Dauphin, P. Liang, and J. Wortman Vaughan, editors, *Advances in Neural Information Processing Systems*, 2021. URL <https://openreview.net/forum?id=2LdBqxc1Yv>.

Qinsheng Zhang and Yongxin Chen. Diffusion normalizing flow. In A. Beygelzimer, Y. Dauphin, P. Liang, and J. Wortman Vaughan, editors, *Advances in Neural Information Processing Systems*, 2021. URL <https://openreview.net/forum?id=x1Lp2b01V1o>.

Pascal Vincent. A connection between score matching and denoising autoencoders. *Neural Computation*, 23(7):1661–1674, 2011. doi:10.1162/NECO_a_00142.

Jiaming Song, Chenlin Meng, and Stefano Ermon. Denoising diffusion implicit models. In *International Conference on Learning Representations*, 2021b. URL <https://openreview.net/forum?id=St1giarCHLP>.

Cheng Lu, Yuhao Zhou, Fan Bao, Jianfei Chen, Chongxuan Li, and Jun Zhu. DPM-solver: A fast ODE solver for diffusion probabilistic model sampling in around 10 steps. *Advances in Neural Information Processing Systems*, 35:5775–5787, 2022b.

Majdi Hassan, Nikhil Shenoy, Jungyoon Lee, Hannes Stark, Stephan Thaler, and Dominique Beaini. Equivariant flow matching for molecular conformer generation. In *ICML’24 Workshop ML for Life and Material Science: From Theory to Industry Applications*, 2024. URL <https://openreview.net/forum?id=zu48fPRYjr>.

R. Ramakrishnan, P. O. Dral, M. Rupp, and O. A. von Lilienfeld. Quantum chemistry structures and properties of 134 kilo molecules. *Scientific Data*, 1(1):140022, 2014. doi:10.1038/sdata.2014.22.

Cheng Lu, Yuhao Zhou, Fan Bao, Jianfei Chen, Chongxuan Li, and Jun Zhu. DPM-Solver++: Fast Solver for Guided Sampling of Diffusion Probabilistic Models, May 2023. URL <http://arxiv.org/abs/2211.01095>. arXiv:2211.01095 [cs].

Martin Heusel, Hubert Ramsauer, Thomas Unterthiner, Bernhard Nessler, and Sepp Hochreiter. Gans trained by a two time-scale update rule converge to a local nash equilibrium. In I. Guyon, U. Von Luxburg, S. Bengio, H. Wallach, R. Fergus, S. Vishwanathan, and R. Garnett, editors, *Advances in Neural Information Processing Systems*, volume 30. Curran Associates, Inc., 2017. URL https://proceedings.neurips.cc/paper_files/paper/2017/file/8a1d694707eb0fefe65871369074926d-Paper.pdf.

Alex Krizhevsky. Learning multiple layers of features from tiny images. Technical Report 0, University of Toronto, Toronto, Ontario, 2009. URL <https://www.cs.toronto.edu/~kriz/learning-features-2009-TR.pdf>.

Tero Karras, Samuli Laine, and Timo Aila. A style-based generator architecture for generative adversarial networks. *2019 IEEE/CVF Conference on Computer Vision and Pattern Recognition (CVPR)*, pages 4396–4405, 2018. URL https://openaccess.thecvf.com/content_CVPR_2019/papers/Karras_A_Style-Based_Generator_Architecture_for_Generative_Adversarial_Networks_CVPR_2019_paper.pdf.

Yunjey Choi, Youngjung Uh, Jaewon Yoo, and Jung-Woo Ha. Stargan v2: Diverse image synthesis for multiple domains. In *Proceedings of the IEEE/CVF Conference on Computer Vision and Pattern Recognition (CVPR)*, June 2020.

Jia Deng, Wei Dong, Richard Socher, Li-Jia Li, Kai Li, and Li Fei-Fei. Imagenet: A large-scale hierarchical image database. In *2009 IEEE Conference on Computer Vision and Pattern Recognition*, pages 248–255, 2009. doi:10.1109/CVPR.2009.5206848.

Bradley Efron. Tweedie’s formula and selection bias. *Journal of the American Statistical Association*, 106(496):1602–1614, 2011. doi:10.1198/jasa.2011.tm11181. URL <https://doi.org/10.1198/jasa.2011.tm11181>. PMID: 22505788.

Simo Särkkä and Arno Solin. *Applied Stochastic Differential Equations*. Cambridge University Press, 1 edition, April 2019. ISBN 978-1-108-18673-5. doi:10.1017/9781108186735. URL <https://www.cambridge.org/core/product/identifier/9781108186735/type/book>.

A Derivation of TV/SNR Expressions of Existing Schedules

In this section, we show the derivations of the TV, $\tau(t)$, and SNR, $\gamma(t)$, for existing diffusion model schedules, which are summarized in Table A1.

A.1 Variance-Exploding (VE) Schedules

Given is the VE perturbation kernel, originally introduced by Song and Ermon [2019] as Denoising Score Matching with Langevin Dynamics (SMLD) and then reframed in the SDE framework by Song et al. [2021a] as VE-SDE,

$$p(\mathbf{x}(t)|\mathbf{x}(0)) = \mathcal{N}(\mathbf{x}(t); \mathbf{x}(0), b^2(t)\mathbf{I}) \quad (15)$$

with

$$a(t) = 1, \quad (16)$$

$$b^2(t) = \sigma_{\min}^2 \left(\frac{\sigma_{\max}}{\sigma_{\min}} \right)^{2t}. \quad (17)$$

Here, σ_{\min} and σ_{\max} are the minimum and maximum noise scales, respectively.

SNR:

$$\gamma^2(t) = \frac{a^2(t)}{b^2(t)} = \frac{1}{\sigma_{\min}^2 \left(\frac{\sigma_{\max}}{\sigma_{\min}} \right)^{2t}} = \sigma_{\min}^{-2} \left(\frac{\sigma_{\min}}{\sigma_{\max}} \right)^{2t}. \quad (18)$$

TV:

$$\begin{aligned} \tau^2(t) &= a^2(t) + b^2(t) \\ &= 1 + \sigma_{\min}^2 \left(\frac{\sigma_{\max}}{\sigma_{\min}} \right)^{2t}. \end{aligned} \quad (19)$$

A.2 Elucidating Design Space of Diffusion Models (EDM)

EDM [Karras et al., 2022] introduces a noise schedule with a scaling factor $s(t)$ and noise level $\sigma(t)$. The perturbation kernel is

$$p(\mathbf{x}(t)|\mathbf{x}(0)) = \mathcal{N}(\mathbf{x}(t); s(t)\mathbf{x}(0), [s(t)\sigma(t)]^2\mathbf{I}) \quad (20)$$

where they use,

$$a(t) = s(t) = 1, \quad (21)$$

$$b^2(t) = \sigma^2(t). \quad (22)$$

The time discretization (7) of the original EDM is illustrated in Figure A1.

SNR:

$$\gamma^2(t) = \frac{a^2(t)}{b^2(t)} = \frac{1}{\sigma^2(t)}. \quad (23)$$

TV:

$$\begin{aligned} \tau^2(t) &= a^2(t) + b^2(t) \\ &= 1 + \sigma^2(t). \end{aligned} \quad (24)$$

A.3 Optimal Transport Flow Matching (FM)

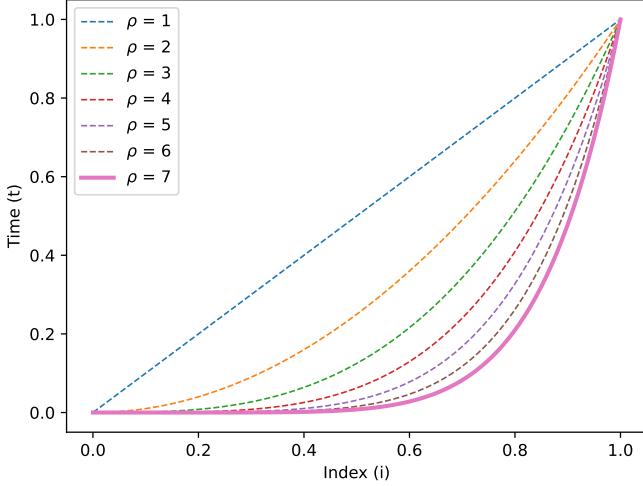
The perturbation kernel of OTFM [Liu et al., 2023b, Lipman et al., 2023] is given by:

$$p_t(\mathbf{x}_t|\mathbf{x}_0) = \mathcal{N}(\mathbf{x}(t); (1-t)\mathbf{x}(0), ((1-t)\sigma_{\min} + t)^2\mathbf{I}) \quad (25)$$

where σ_{\min} is sufficiently small, resulting in a Gaussian distribution concentrated around $x(0)$. Assuming $\sigma_{\min} = 0$ and incorporating the boundary constraint on $t \in [\varepsilon_{\min}, 1]$, we can define:

Table A1: TV $\tau(t)$ and SNR $\gamma(t)$ schedules corresponding to commonly used diffusion processes within our framework.

Method	$\tau^2(t)$	$\gamma^2(t)$	time grid
SMLD [Song and Ermon, 2019]	$1 + \sigma_{\min}^2 \left(\frac{\sigma_{\max}}{\sigma_{\min}} \right)^{2t}$	$\sigma_{\min}^{-2} \left(\frac{\sigma_{\min}}{\sigma_{\max}} \right)^{2t}$	uniform
EDM [Karras et al., 2022]	$1 + \sigma^2(t)$	$\sigma^{-2}(t)$	Eq.(7)
EDM-UT	$1 + \left(\sigma_{\max}^{\frac{1}{\rho}} + (1-t) \left(\sigma_{\min}^{\frac{1}{\rho}} - \sigma_{\max}^{\frac{1}{\rho}} \right) \right)^{2\rho}$	$\left(\sigma_{\max}^{\frac{1}{\rho}} + (1-t) \left(\sigma_{\min}^{\frac{1}{\rho}} - \sigma_{\max}^{\frac{1}{\rho}} \right) \right)^{-2\rho}$	uniform
OTFM [Lipman et al., 2023]	$1 - 2t(1-t)$	$(\frac{1}{t} - 1)^2$	uniform
DDPM-linear [Ho et al., 2020]	1	$\left(e^{\frac{1}{2}t^2(\beta_{\max} - \beta_{\min}) + t\beta_{\min}} - 1 \right)^{-1}$	uniform
DDPM-cos [Nichol and Dhariwal, 2021]	1	$\left(\left(\frac{\cos(\frac{s}{1+s} \frac{\pi}{2})}{\cos(\frac{t\nu+s}{1+s} \frac{\pi}{2})} \right)^2 - 1 \right)^{-1}$	uniform
VP-SMLD (Ours)	1	$\sigma_{\min}^{-2} \left(\frac{\sigma_{\min}}{\sigma_{\max}} \right)^{2t}$	uniform
VP-EDM-UT (Ours)	1	$\left(\sigma_{\max}^{\frac{1}{\rho}} + (1-t) \left(\sigma_{\min}^{\frac{1}{\rho}} - \sigma_{\max}^{\frac{1}{\rho}} \right) \right)^{-2\rho}$	uniform
VP-OTFM (Ours)	1	$(\frac{1-t}{t})^2$	uniform
VP-ISSNR (Ours)	1	$(\frac{1-t}{t})^{2\eta} \exp(2\kappa)$	uniform

Figure A1: The time discretization (7) of the original EDM sampler [Karras et al., 2022] for various parameters ρ . At $\rho = 1$, linear time discretization is recovered, i.e. $t(i) = i$. For larger ρ , time steps get considerably shorter close to the data distribution. EDM uses $\rho = 7$.**SNR:**

$$\gamma^2(t) = \frac{(1-t)^2}{t^2} = \left(\frac{1}{t} - 1 \right)^2. \quad (26)$$

TV:

$$\tau^2(t) = (1-t)^2 + t^2 = 1 - 2t(1-t). \quad (27)$$

A.4 Denoising Diffusion Probabilistic models (DDPM)

The original DDPM model [Ho et al., 2020] used the perturbation kernel:

$$p(\mathbf{x}(t)|\mathbf{x}(0)) = \mathcal{N} \left(\mathbf{x}(t); \sqrt{\bar{\alpha}(t)}\mathbf{x}(0), (1 - \bar{\alpha}(t))\mathbf{I} \right) \quad (28)$$

SNR

$$\gamma^2(t) = \frac{a^2(t)}{b^2(t)} = \frac{\bar{\alpha}(t)}{1 - \bar{\alpha}(t)}. \quad (29)$$

TV

$$\begin{aligned} \tau^2(t) &= a^2(t) + b^2(t) \\ &= 1. \end{aligned} \quad (30)$$

While the TV is always constant in the VP case, different schedules were adopted for $\bar{\alpha}(t)$. The most common are:

- **DDPM-linear** the original linear schedule introduced by Ho et al. [2020] and adopted by Song et al. [2021a] as VP-SDE, where:

$$\bar{\alpha}(t) = e^{-\frac{1}{2}t^2(\beta_{\max} - \beta_{\min}) - t\beta_{\min}},$$

and therefore

$$\begin{aligned} \gamma^2(t) &= \frac{e^{-\frac{1}{2}t^2(\beta_{\max} - \beta_{\min}) - t\beta_{\min}}}{1 - e^{-\frac{1}{2}t^2(\beta_{\max} - \beta_{\min}) - t\beta_{\min}}} \\ &= \left(\frac{1 - e^{-\frac{1}{2}t^2(\beta_{\max} - \beta_{\min}) - t\beta_{\min}}}{e^{-\frac{1}{2}t^2(\beta_{\max} - \beta_{\min}) - t\beta_{\min}}} \right)^{-1} \\ &= \left(e^{\frac{1}{2}t^2(\beta_{\max} - \beta_{\min}) + t\beta_{\min}} - 1 \right)^{-1}. \end{aligned} \quad (31)$$

- **DDPM-cos** First introduced by Nichol and Dhariwal [2021] as a better alternative to the linear schedule:

$$\bar{\alpha}(t) = \frac{u(t)}{u(0)}, \quad \text{where} \quad u(t) = \cos \left(\frac{t^\nu + s \pi}{1+s} \frac{\pi}{2} \right)^2.$$

Note that the parameter ν does not exist in the original formulation [Nichol and Dhariwal, 2021] but we adopt it from Vignac et al. [2023]. The SNR is therefore:

$$\begin{aligned} \gamma^2(t) &= \frac{u(t)}{u(0) \left(1 - \frac{u(t)}{u(0)} \right)} \\ &= \frac{u(t)}{u(0) - u(t)} \\ &= \left(\frac{u(0)}{u(t)} - 1 \right)^{-1} \\ &= \left(\left(\frac{\cos \left(\frac{s \pi}{1+s} \frac{\pi}{2} \right)}{\cos \left(\frac{t^\nu + s \pi}{1+s} \frac{\pi}{2} \right)} \right)^2 - 1 \right)^{-1}. \end{aligned} \quad (32)$$

B Derivation of the SDE

B.1 Derivation of the perturbation kernel for a given affine SDE

As shown by Song et al. [2021a], a diffusion process can be described by a continuous stochastic differential equation (SDE) describing an Itô process:

$$d\mathbf{x} = \mathbf{f}(\mathbf{x}, t) dt + \mathbf{g}(\mathbf{x}, t) d\mathbf{w}, \quad (33)$$

where \mathbf{x} is the state variable, \mathbf{w} is the standard Wiener process, and $\mathbf{f}(\mathbf{x}, t)$ and $\mathbf{g}(\mathbf{x}, t)$ are predefined functions describing the drift and diffusion coefficients, respectively.

While Song et al. [2021a] derived the perturbation kernel using the differential equations for the mean and covariance of an SDE, we take a different approach. By exploiting the affine nature of the SDE in our case, we first solve the SDE and then derive the perturbation kernel parameters, arriving at the same solution. Specifically, for the affine case where

$$d\mathbf{x} = f(t)\mathbf{x} dt + g(t) d\mathbf{w}, \quad (34)$$

the integral of the Itô process is described by Eq. (4.28) in Särkkä and Solin [2019] as

$$\mathbf{x}(t) = \phi(t, 0)\mathbf{x}(0) + \int_0^t \phi(t, s)g(s) d\mathbf{w}(s) \quad (35)$$

with an integrating factor $\phi(t, s)$ and initial condition $\mathbf{x}(0)$. In the following we use the integrating factor $\phi(t, s) = \exp\left(\int_s^t f(u) du\right)$.

The solution $\mathbf{x}(t)$ involves a deterministic part dependent on $\mathbf{x}(0)$ and a stochastic part independent of $\mathbf{x}(0)$ and involving a standard Wiener process. Thus, we can derive a Gaussian perturbation kernel for this process following the general form defined in Eq. (1):

$$\begin{aligned} a(t)\mathbf{x}(0) &= \mathbb{E}[\mathbf{x}(t)|\mathbf{x}(0)] \\ &= \mathbb{E}[\phi(t, 0)\mathbf{x}(0)|\mathbf{x}(0)] + \underbrace{\mathbb{E}\left[\int_0^t \phi(t, s)g(s) d\mathbf{w}(s)|\mathbf{x}(0)\right]}_{=0, \text{ since } \mathbb{E}[d\mathbf{w}]=0} \\ &= \phi(t, 0)\mathbf{x}(0), \end{aligned}$$

and

$$\begin{aligned} b^2(t) &= \text{Var}(\mathbf{x}(t)|\mathbf{x}(0)) \\ &= \underbrace{\text{Var}(\phi(t, 0)\mathbf{x}(0)|\mathbf{x}(0))}_{=0} + \text{Var}\left(\int_0^t \phi(t, s)g(s) d\mathbf{w}(s)|\mathbf{x}(0)\right) \\ &= \mathbb{E}\left[\left(\int_0^t \phi(t, s)g(s) d\mathbf{w}(s)\right)^2|\mathbf{x}(0)\right] + \underbrace{\left(\mathbb{E}\left[\int_0^t \phi(t, s)g(s) d\mathbf{w}(s)|\mathbf{x}(0)\right]\right)^2}_{=0, \text{ since } \mathbb{E}[d\mathbf{w}]=0} \\ &\stackrel{\text{(Itô isometry)}}{=} \mathbb{E}\left[\int_0^t \phi(t, s)^2 g(s)^2 ds|\mathbf{x}(0)\right] \\ &= \int_0^t \phi(t, s)^2 g(s)^2 ds. \end{aligned}$$

Summarizing, the perturbation kernel parameters are given by:

$$a(t) = \phi(t, 0) = \exp\left(\int_0^t f(u) du\right), \quad (36)$$

$$b^2(t) = \int_0^t \phi(t, s)^2 g(s)^2 ds = \int_0^t \exp\left(2 \int_s^t f(u) du\right) g(s)^2 ds. \quad (37)$$

B.2 Derivation of the SDE for a given perturbation kernel

In the previous section (Appendix B.1), we derived a perturbation kernel with the general form specified in Eq. (1) from a given SDE. In this section, we do the opposite and derive the SDE that results in a given perturbation kernel, where we use

the results from the previous section. Starting from the definition of $a(t)$ in Eq. (36) and $b^2(t)$ in Eq. (37), we can first derive the drift $f(t)$ of the affine SDE (Eq. (34)):

$$\begin{aligned} \exp \left(\int_0^t f(u) du \right) &= a(t) \\ \therefore f(t) &= \frac{d[\log a(t)]}{dt} = \frac{\dot{a}(t)}{a(t)}. \end{aligned}$$

where $\dot{a}(t) = \frac{d[a(t)]}{dt}$ denotes the derivative of $a(t)$ with respect to time. Next, we derive the diffusion coefficient $g(t)$:

$$\begin{aligned} b^2(t) &= \int_0^t \exp \left(2 \int_s^t f(u) du \right) g(s)^2 ds \\ &= \int_0^t \exp \left(2 \int_s^t \frac{d[\log a(u)]}{du} du \right) g(s)^2 ds \\ &= \int_0^t \exp (2 (\log a(t) - \log a(s))) g(s)^2 ds \\ &= \int_0^t \frac{a(t)^2}{a(s)^2} g(s)^2 ds \\ &= a^2(t) \int_0^t \frac{g(s)^2}{a(s)^2} ds \\ \therefore \left(\frac{b(t)}{a(t)} \right)^2 &= \int_0^t \frac{g(s)^2}{a(s)^2} ds. \end{aligned}$$

Deriving both sides with respect to t and solving for $g(t)$, we get

$$\begin{aligned} \frac{g(t)^2}{a(t)^2} &= 2 \frac{b(t)}{a(t)} \frac{d}{dt} \left(\frac{b(t)}{a(t)} \right) \\ \therefore g(t) &= \sqrt{2 a(t) b(t) \frac{d}{dt} \left(\frac{b(t)}{a(t)} \right)}. \end{aligned}$$

Thus, the SDE parameters are given by

$$f(t) = \frac{d[\log a(t)]}{dt} = \frac{\dot{a}(t)}{a(t)}, \quad (38)$$

$$g(t) = \sqrt{2 a(t) b(t) \frac{d}{dt} \left(\frac{b(t)}{a(t)} \right)}. \quad (39)$$

When defining the perturbation kernel to explicitly include a scaling factor, i.e., when $b^2(t) = a^2(t) c(t)^2$, $p(\mathbf{x}(t)|\mathbf{x}(0)) = \mathcal{N}(\mathbf{x}(t); a(t)\mathbf{x}_0, a^2(t) c(t)^2 \mathbf{I})$ and therefore $\tilde{\mathbf{x}}(t) = (\mathbf{x}(t)/a(t)) \sim \mathcal{N}(\mathbf{x}_0, c(t)^2 \mathbf{I})$, we get the special case of Eq. (39):

$$g(t) = \sqrt{2 a(t) a(t) c(t) \frac{d}{dt} \left(\frac{a(t) c(t)}{a(t)} \right)} = a(t) \sqrt{2 c(t) \dot{c}(t)} \quad (40)$$

B.3 Derivation of our TV/SNR SDE

Using the results from sections B.1 and B.2, we derive our TV/SNR SDE. To this end, we first define the perturbation kernel as

$$p(\mathbf{x}(t)|\mathbf{x}(0)) = \mathcal{N} \left(\mathbf{x}(t); \sqrt{\frac{\tau^2(t) \gamma^2(t)}{1 + \gamma^2(t)}} \mathbf{x}(0), \frac{\tau^2(t)}{1 + \gamma^2(t)} \mathbf{I} \right). \quad (41)$$

Given the TV/SNR perturbation kernel in Eq. (41) and the results from Appdix B.2, we can derive the SDE that results in this perturbation kernel. First, using Eq. (38) we derive $f(t)$, where

$$a^2(t) = \frac{\tau^2(t)\gamma^2(t)}{1 + \gamma^2(t)}.$$

Abbreviating as $\tau = \tau(t)$ and $\gamma = \gamma(t)$ to avoid clutter, we have

$$\frac{d}{dt}a(t)^2 = 2\dot{a}(t)a(t)$$

and

$$\begin{aligned} \frac{d}{dt}a(t)^2 &= \frac{d}{dt}\left(\frac{\tau^2\gamma^2}{1 + \gamma^2}\right) = \frac{(1 + \gamma^2)(2\tau\dot{\gamma}^2 + 2\gamma\dot{\gamma}\tau^2) - \tau^2\gamma^2(2\gamma\dot{\gamma})}{(1 + \gamma^2)^2} \\ &= \frac{2\tau\dot{\gamma}\gamma^2(1 + \gamma^2) + 2\gamma\dot{\gamma}\tau^2}{(1 + \gamma^2)^2}. \end{aligned}$$

Therefore

$$\begin{aligned} \dot{a}(t) &= \frac{\frac{d}{dt}a^2(t)}{2a(t)} \\ &= \frac{\tau\dot{\gamma}\gamma^2(1 + \gamma^2) + \gamma\dot{\gamma}\tau^2}{a(t)(1 + \gamma^2)^2} \end{aligned}$$

and

$$\begin{aligned} f(t) &= \frac{\dot{a}(t)}{a(t)} \\ &= \frac{\tau\dot{\gamma}\gamma^2(1 + \gamma^2) + \gamma\dot{\gamma}\tau^2}{a^2(t)(1 + \gamma^2)^2} \\ &= \frac{\tau\dot{\gamma}\gamma^2(1 + \gamma^2) + \gamma\dot{\gamma}\tau^2}{\tau^2\gamma^2(1 + \gamma^2)}. \end{aligned}$$

Consequently we have

$$f(t) = \frac{\dot{\tau}(t)}{\tau(t)} + \frac{\dot{\gamma}(t)}{\gamma(t)(1 + \gamma^2(t))}. \quad (42)$$

Now, we can derive the diffusion coefficient $g(t)$, where we can use the special case of Eq. (39), when the variance is explicitly scaled by the mean factor $a(t)$:

$$\begin{aligned} b^2(t) &= a^2(t)c(t)^2 = \frac{\tau^2(t)\gamma^2(t)}{1 + \gamma^2(t)} \frac{1}{\gamma^2(t)} \\ &\Rightarrow c(t) = \gamma(t)^{-1}. \end{aligned}$$

Thus, we use Eq. (40) to solve for $g(t)$, where

$$\dot{c}(t) = \frac{d}{dt}(\gamma(t)^{-1}) = -\frac{\dot{\gamma}(t)}{\gamma^2(t)}$$

and hence

$$\begin{aligned} g(t) &= a(t)\sqrt{2c(t)\dot{c}(t)} \\ &= \sqrt{\frac{\tau^2(t)\gamma^2(t)}{1 + \gamma^2(t)}} \sqrt{-2\frac{1}{\gamma(t)}\frac{\dot{\gamma}(t)}{\gamma^2(t)}} \\ &= \sqrt{\frac{-2\tau^2(t)\dot{\gamma}(t)}{\gamma(t)(1 + \gamma^2(t))}}. \end{aligned} \quad (43)$$

Note that $\gamma(t)$ needs to be differentiable, monotonically decreasing and positive for all $t \in [0, 1]$ to ensure that the SDE is well-defined, i.e., the square root in the diffusion coefficient $g(t)$ is well-defined and the dominant term in the drift $f(t)$ is non-zero.

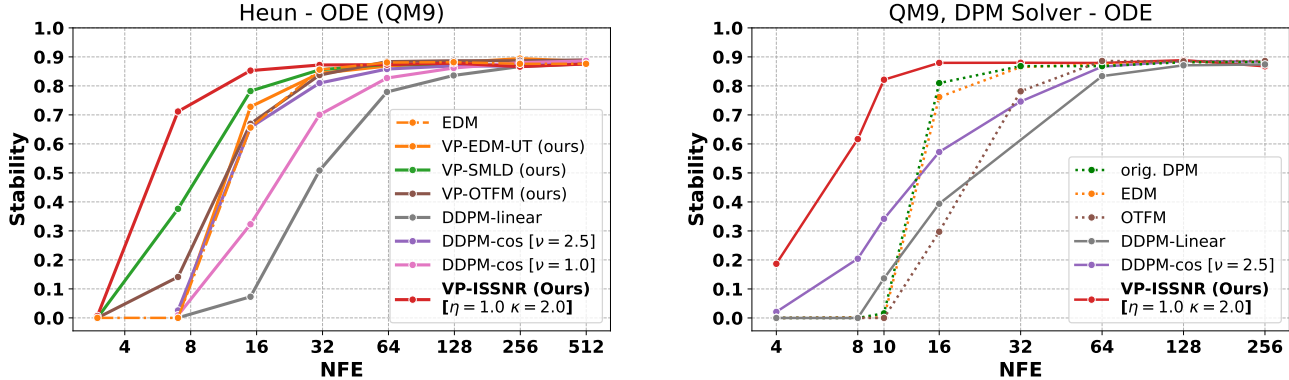


Figure A2: Stability rate (**higher is better**) as a function of the number of function evaluations (NFE) for molecular structure generation on the QM9 dataset, using the second-order Heun sampler (**left**) and the DPM solver [Lu et al., 2022a, 2023] (**right**).

C Experimental Details

For training a diffusion model, we use the loss in Eq. (5) to keep a unit variance of the model output for all t , and adopt the same noise model architecture ε_θ from Kahouli et al. [2024], but use 9 interaction blocks, train on continuous time and condition the model on a scaled SNR instead of the time t , i.e., $\varepsilon_\theta(\hat{\mathbf{x}}(t), c_{\text{snr}}(\gamma^2(t)))$, where $\hat{\mathbf{x}}(t)$ is a scaled version of $\mathbf{x}(t)$ to unit variance. This is achieved by first scaling the training data by σ_{data} , which is approximately $\sqrt{2}$ for the QM9 dataset, and always setting $\tau(t) = 1$ during training, independent of the training SNR schedule. This has the benefit of making the model compatible with various TV and SNR schedules during sampling without retraining, and avoiding model stability issues due to large cutoff distances in the Graph Neural Network when using non-constant $\tau(t)$. We define $c_{\text{snr}}(\gamma^2(t)) = \omega \log(\gamma^2(t)) + \xi$ to linearize the SNR input, keeping it in a stable, normalized range, with $\omega = 0.35$ and $\xi = -0.125$ providing good performance. During sampling with a TV schedule $\tau(t) \neq 1$, we scale the model input to $\hat{\mathbf{x}}(t) = \tau(t)^{-1} \mathbf{x}(t)$ to maintain unit variance for all t . Note that the reverse trajectory itself will not become constant. The generated samples $\mathbf{x}(0)$ are then scaled back to the target data variance by multiplying by σ_{data} .

We tuned t_{max} such that $\gamma(t)^{-1}$ approximates the dataset’s maximum pairwise Euclidean distance. For molecules with different number of atoms we choose the average. This ensures that all the modes of the distribution are mixed at t_{max} . We tune t_{min} to the largest value producing almost noiseless samples, avoiding extra reverse steps near the data manifold.

We trained two models using different schedules: (i) DDPM-cos with $\nu = 1.0$ and (ii) the EDM SNR schedule with $\tau(t) = 1$ for the reasons discussed before. We then sampled from each model using all schedules and found that the model trained with DDPM-cos consistently outperformed the EDM-trained model, even when using the EDM schedule for sampling, as depicted in Figure A4. Therefore, we report only the results using the model trained on the DDPM-cos in the main text, while results for the model trained on the EDM schedule are included in Appendix D.

D Additional Experimental Results

D.1 Molecular structure generation

Figure A2 shows the stability rate of the generated molecular structures with the second-order integration method, Heun, and the advanced DPM solver [Lu et al., 2022a, 2023]. We observe only a marginal improvement with high NFEs, compared to the performance achieved by Euler in Figure 3. However, the same trend between schedules is observed for different samplers, supporting the hypothesis that improvements in sampling methods and noise schedules are orthogonal to each other, i.e., they can be combined for even greater overall improvements.

Figure A3 shows molecular structure generation performance evaluated by running DFT to relax the generated structures, which further validates the stability rate results (we observe a similar trend with this evaluation criterion).

Figure A4 compares the sample generation performance with the diffusion model trained on different schedules, DDPM-cosine with $\nu = 1$ and EDM. We can see that the model trained on the cosine schedule achieves consistently better results than the model trained on the EDM schedule, even when using the EDM schedule during sampling. This suggests that the cosine schedule samples more points on the relevant SNR region.

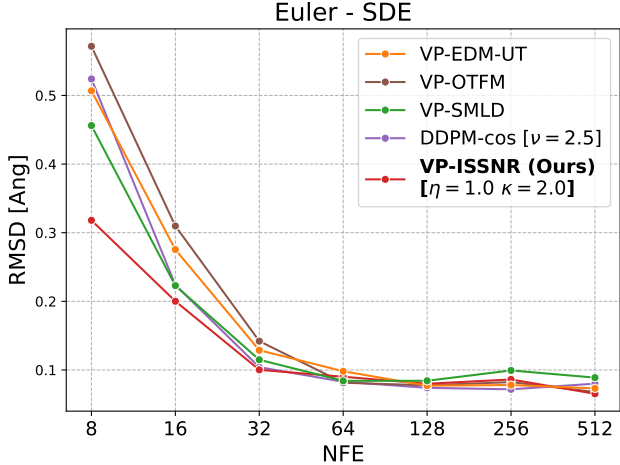


Figure A3: Root mean square deviation (RMSD, **lower is better**) between the generated structures and reference structures obtained from geometry relaxations using DFT calculations at the B3LYP/6-31G(2df,p) level of theory, the same method used for generating the structures in QM9 [Ramakrishnan et al., 2014], which the model was trained on. We see a similar trend to the stability rate results in Figure 3, where our VP-ISSNR consistently outperforms other approaches. This reveals that our method can generate physically plausible molecules that are structurally similar to ground truth reference structures.

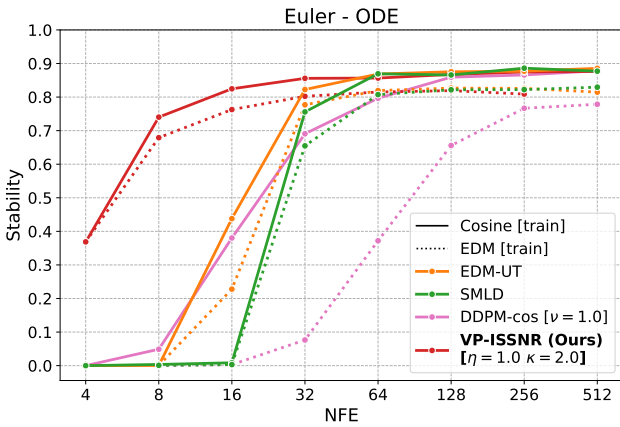


Figure A4: Effect of the schedule used during training. Using the same schedule for both training and sampling does not enhance results for EDM, whereas the Cosine schedule emphasizes sampling in more challenging regions during training. Our VP-ISSNR sampling still outperforms other baselines, even when the model is trained using the EDM schedule.

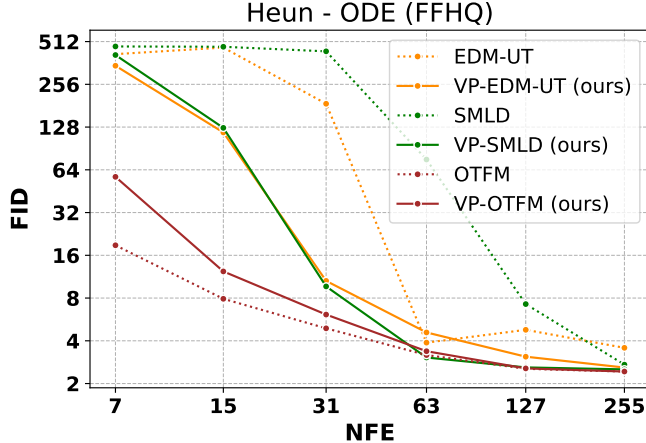


Figure A5: FID score (**lower is better**) as a function of the number of function evaluations (NFE) in image generation on FFHQ, comparing existing non-VP schedules with their VP variants.

D.2 Image Generation

For a more rigorous benchmarking of our approach, we further present the following experimental results:

Figure A5 compares existing non-VP with their VP variants in image generation on FFHQ.

Figure A6 compares the results of using different solvers with different noise schedules, including the VP-ISSNR variant with fixed hyperparameters for completeness. The results further supports the hypothesis that improvements in the sampler/solver are orthogonal to improvements in the noise schedule and can be combined for even greater overall improvement.

Figure A7 investigates the robustness and generalizability of different schedules, including the VP-ISSNR variant with fixed hyperparameters, to different image datasets with different resolutions. Overall, we can observe the same trade-off across datasets, with our tuned schedule reaching the lowest FID score.

D.3 Trajectory Analysis

Extending the subset of trajectories shown in Figure 1, in Figure A8, we show the ODE trajectories for all the noise schedules that were used in Section 4.

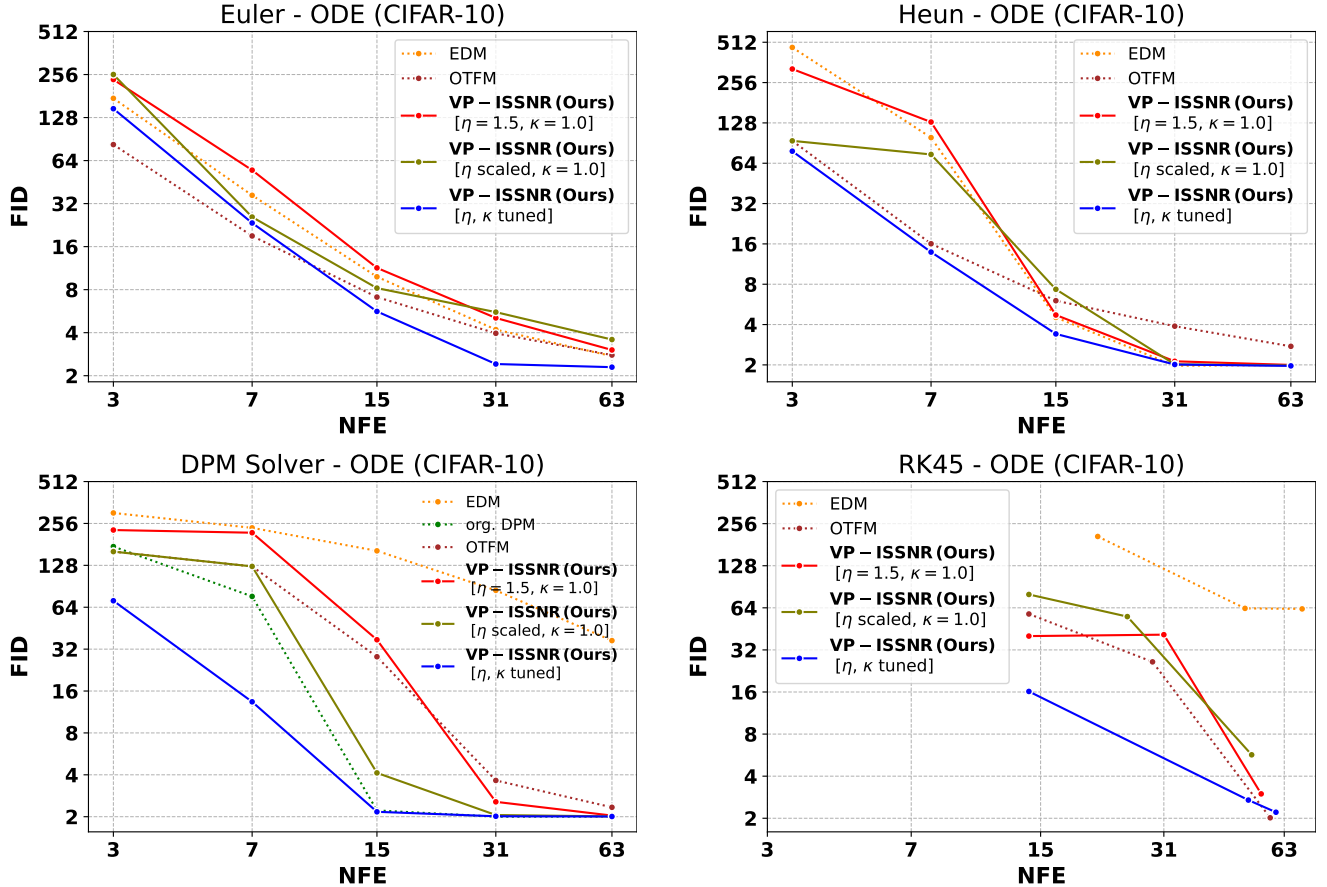


Figure A6: FID score (**lower is better**) as a function of the number of function evaluations (NFE) for image generation on CIFAR10. Results are shown for a combinations of solvers and noise schedules, including the VP-ISSNR variant with fixed hyperparameters in red. Solvers include Euler (first-order), Heun (second-order), RK45 (high-order), and the advanced DPM solver Lu et al. [2022a, 2023]. For the DPM solver, their proposed schedule is indicated in green. Due to the difficulty of precisely controlling the NFE for RK45, some data points may be missing or slightly shifted in the plot.

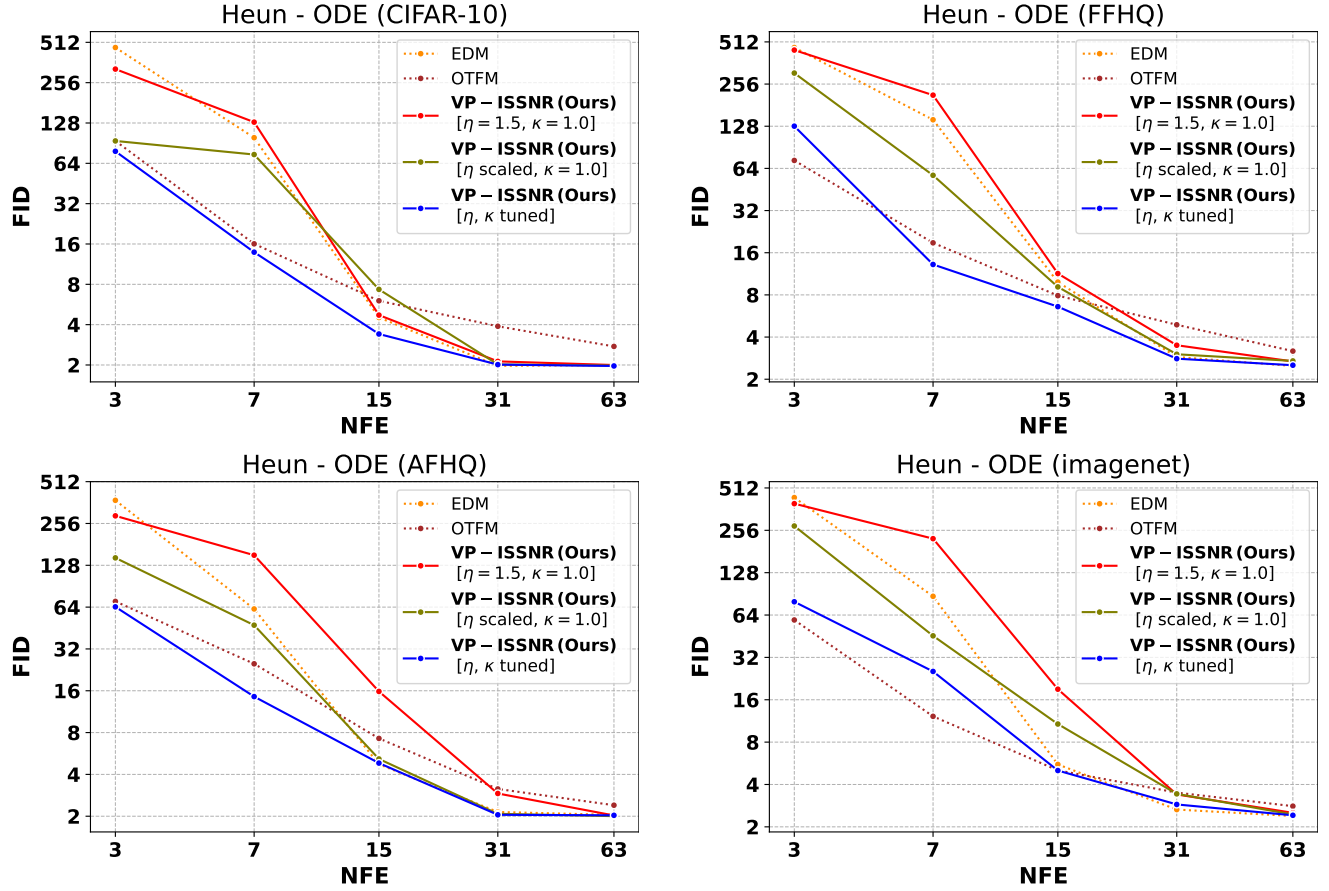


Figure A7: FID score (**lower is better**) as a function of the number of function evaluations (NFE) for image generation using different datasets with different image resolutions and the second-order solver Heun. For completeness, we add the results of using the fixed hyperparameters variant of our VP-ISSNR schedule in red.

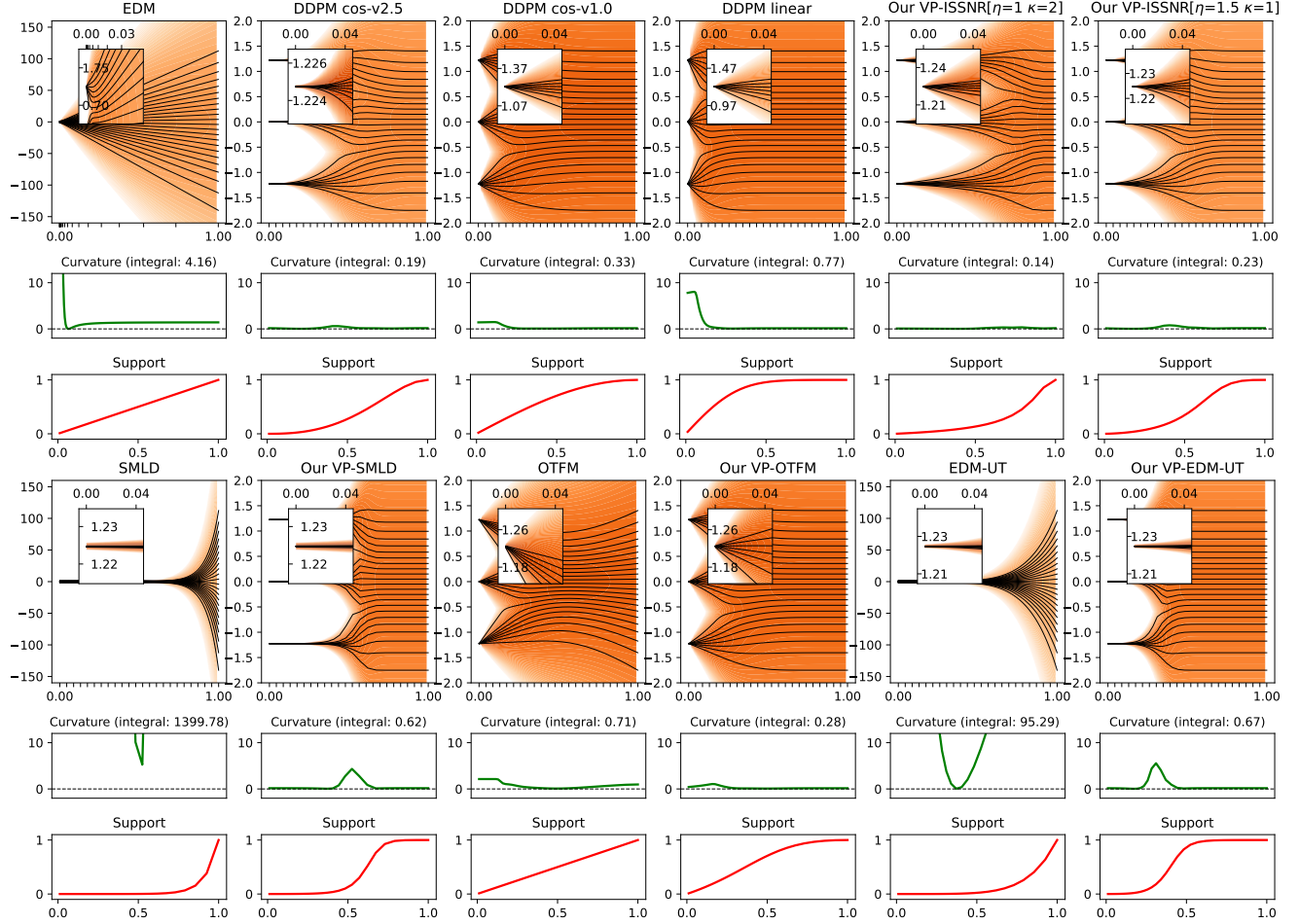


Figure A8: ODE trajectories (black solid curves) and the marginal density path (orange shadows) when the data distribution is a mixture of three uniformly spaced delta peaks. The insets focus on the neighborhood of one of the peaks at $x = \frac{3}{2}$ and $t \ll 1$, and the green and red curves indicate the local curvature and the support (relative to the one at $t = 1$), respectively. On top of the green curve, we report the global curvature integrated over t .